Stability of the Rankine vortex in a multipolar strain field

Christophe Eloy and Stéphane Le Dizès

Institut de Recherche sur les Phénomènes Hors Équilibre, Technopôle de Château-Gombert,
49 rue F. Joliot Curie, BP 146, 13384 Marseille cedex 13, France

In this paper, the linear stability of a Rankine vortex in an *n*-fold multipolar strain field is addressed. The flow geometry is characterized by two parameters: the degree of azimuthal symmetry *n* which is an integer and the strain strength ε which is assumed to be small. For $n=2$, 3 and 4 (dipolar, tripolar and quadrupolar strain fields, respectively), it is shown that the flow is subject to a three-dimensional instability which can be described by the resonance mechanism of Moore and Saffman [Proc. R. Soc. London, Ser. A **346**, 413 (1975)]. In each case, two normal modes (Kelvin modes), with the azimuthal wave numbers separated by *n*, resonate and interact with the multipolar strain field when their axial wave numbers and frequencies are identical. The inviscid growth rate of each resonant Kelvin mode combination is computed and compared to the asymptotic values obtained in the large wave numbers limits. The instability is also interpreted as a vorticity stretching mechanism. It is shown that the inviscid growth rate is maximum when the perturbation vorticity is preferentially aligned with the direction of stretching. Viscous effects are also considered for the distinguished scalings: $\nu=O(\varepsilon)$ for $n=2$ and 3, $\nu=O(\varepsilon^2)$ for $n=4$, where ν is the dimensionless viscosity. The instability diagram showing the most unstable mode combination and its growth rate as a function of viscosity is obtained and used to discuss the role of viscosity in the selection process. Interestingly, for $n=2$ in a high viscosity regime, a combination of Kelvin modes of azimuthal wave numbers $m=0$ and $m=2$ is found to be more unstable than the classical helical modes $m=\pm1$. For $n=3$ and 4, the azimuthal structure of the most unstable Kelvin mode combination is shown to be strongly dependent on viscous effects. The results are discussed in the context of turbulence and compared to recent observations of vortex filaments. © *2001 American Institute of Physics.* [DOI: 10.1063/1.1345716]

I. INTRODUCTION

Recent experiments and numerical simulations demonstrate the presence of structures of high vorticity in turbulence (see for instance Refs. 1–3). It was argued that those elongated and distorted filaments of vorticity could play an important role in the intermittent character of turbulence.[4] Arendt *et al.*,[5] in numerical simulations of gravity waves, showed that the deformation of those vortex tubes could be viewed as a superposition of Kelvin modes[6] on a straight filament, but they did not propose a mechanism for the generation of such perturbations. The aim of this paper is to provide such a mechanism.

This paper focuses on the idealized Rankine vortex flow which allows a comprehensive analysis. The vortex is subject to a multipolar potential strain field perpendicular to the vortex axis which induces a deformation of the streamlines in the rotational part of the flow. Our goal is to understand under which conditions Kelvin modes can appear spontaneously on the vortex via a coupling with the multipolar strain. In particular, we want to address the role of viscous and finite core size effects in the Kelvin mode selection process.

The effect of an external perpendicular strain field on a vortex filament is known to induce, at first order, an elliptic deformation of the streamlines.[7–9] The stability of such a deformed filament was first studied by a global analysis in

the context of vortex rings.[10,11] The mechanism of the instability was explained by Tsai and Widnall[12] for an elliptical Rankine vortex and by Moore and Saffman[13] for a general inviscid vorticity profile. They showed that the instability could be interpreted as a resonance phenomenon of the Kelvin modes of the underlying vortex with the elliptic distortion. In particular, they established that the combination of *stationary* helical modes of azimuthal wave numbers $m=-1$ and $m=1$ is always resonant and unstable. The growth of this resonant helical combination leads to a sinuous deformation of the vortex in the plane of maximal positive stretching. So far, there has been no proof that this combination of Kelvin modes is the most unstable, but this is supported by numerous experimental observations.[14–17] In this paper, the growth rate of all possible resonant configurations will be computed. The conditions under which the helical mode combination is the most unstable will be established.

The unstable character of elliptic streamlines was reexamined by Pierrehumbert[18] and Bayly[19] using a local approach. They showed that the instability, called *elliptic instability* in this framework, could be interpreted as a parametric excitation of inertial waves. Lifschitz and Hameiri[20] recovered this result in their general stability theory based on geometrical optics methods. This local theory was also used to
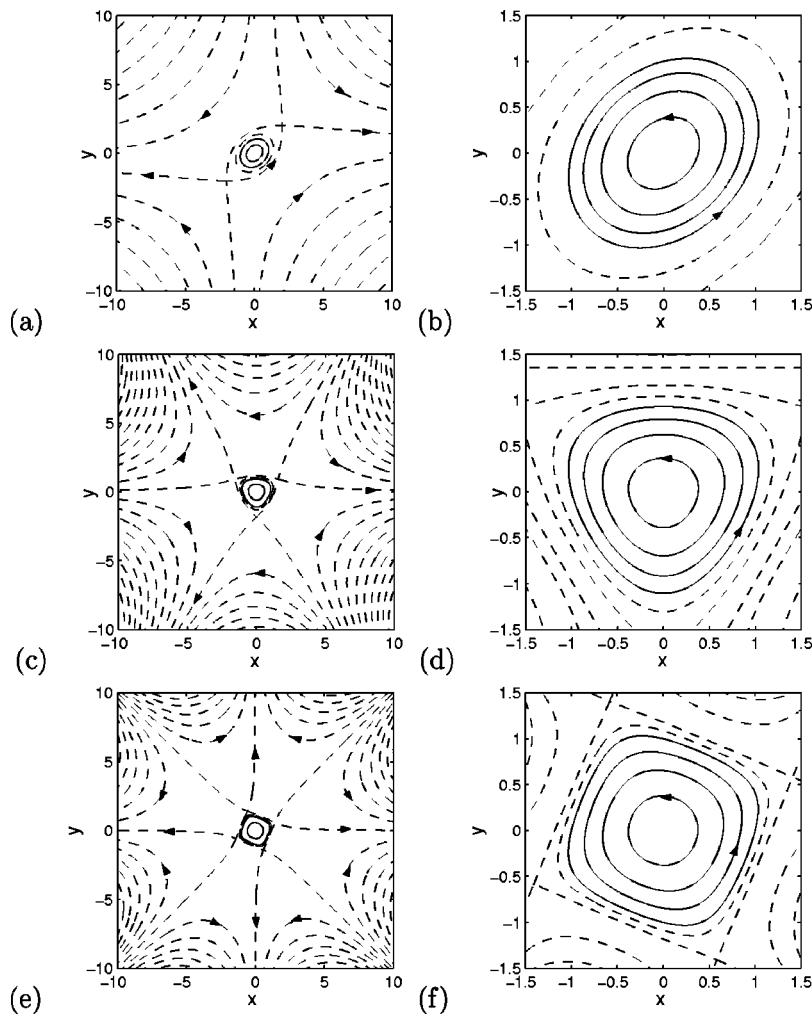
FIG. 1. Streamlines of the Rankine vortex in a multipolar strain field of strength $\varepsilon = 0.25$. The flow given by Eqs. (1.1a) and (1.1b) is pictured at two different scales for dipolar strain field ($n=2$) (a,b), tripolar strain field ($n=3$) (c,d) and quadrupolar strain field ($n=4$) (e,f). The solid and dashed lines are inside and outside the vortex core, respectively.

account for various additional effects such as time dependence, stretching, stratification, etc. (see Bayly et al.[21] and reference therein). The connection between the local and global descriptions of the elliptic instability was made by Waleffe[22] who showed that most unstable inertial waves could be summed up to form the resonant helical Kelvin mode combination of Tsai and Widnall.[12]

Few experimental works have been designed to study the elliptic instability. Chernous'ko[23] studied the flow inside an elliptic cylinder and gave an instability diagram showing the number of structures as a function of aspect ratio and eccentricity. Gledzer and Ponomarev[15] and Malkus[14] confirmed that these results agree with the Kelvin mode resonance mechanism. Experimental observations of the elliptic instability have also been evidenced in open flows configurations such as vortex rings[10] and vortex pairs.[16] It has also been recognized as an important mechanism in the secondary instability transition in shear layers,[24,25] wakes[17] and rotating flows in confined geometry.[26,27]

In this paper, we perform a global stability analysis of the Rankine vortex in a weak stationary multipolar strain field. The basic flow is given by the following streamfunctions [in cylindrical coordinates (r, θ, z)]:

$$\psi_{\text{in}}(r, \theta) = -\frac{1}{2} r^2 + \frac{\varepsilon}{n} r^n \sin(n\theta) + O(\varepsilon^2) \quad \text{for } r \leqslant R,$$

(1.1a)

$$\psi_{\text{out}}(r, \theta) = -\ln(r) + \frac{\varepsilon}{n^2}[(n-1)r^n + r^{-n}]\sin(n\theta)$$

$$+ O(\varepsilon^2) \quad \text{for } r > R,$$

(1.1b)

with $R(\theta)$ such that $\psi_{\text{in}}(R, \theta) = -1/2$, i.e.,

$$R(\theta) = 1 + \frac{\varepsilon}{n}\sin(n\theta) + O(\varepsilon^2),$$

(1.2)

where n is an integer and ε is a small parameter measuring the strength of the external field. Here, the basic rotation speed and the vortex radius have been used to nondimensionalize the variables. This solution is the extension of Moore and Saffman solution[28] to a multipolar strain field in the limit of weak external field. Figure 1 pictures the streamlines of the flow for $\varepsilon = 0.25$ and $n = 2$, 3 and 4. For $n=2$, all the inner streamlines are ellipses with same eccentricity ε. For larger n, the streamlines are circular in the vicinity of the center and become more deformed close to $r = R(\theta)$. The case of pure strain field ($n=2$) was considered by Tsai and

Widnall.[12] Our goal is here twofold. First, we want to reconsider the pure strain case to show that other unstable modes different from the helical mode combinations obtained by Tsai and Widnall exist and that they may become dominant if viscosity is included. Second, we want to show that a similar instability mechanism exists when the pure strain is replaced by a multipolar strain field which corresponds to a higher symmetrical environment (network of vortices, vortex in a square box).

In a previous paper,[29] we addressed the local stability of the streamlines defined by Eq. (1.1a) using the Lifschitz and Hameiri theory.[20] The results can be summarized as follows. For $n=2$, 3 and 4, a given closed streamline $\psi_{in}=C$ is unstable with respect to short wavelength inviscid perturbations as soon as $\varepsilon>0$ with a leading order growth rate proportional to the asymmetry parameter $\varepsilon_n \equiv \varepsilon [2nC/(2-n)]^{(n-2)/2}$. For $n \geq 5$, the streamlines become unstable only if they are sufficiently distorted, i.e., if ε_n is above a positive critical value. With the restrictions $-1/2 \leq C \leq 0$ and small ε, one then expects the flow to be locally unstable for $n=2$, 3 and 4 with a maximum inviscid growth rate given by $\sigma=(9/16)\varepsilon$, $(49/32)\varepsilon$ and 3ε, respectively, and locally stable for larger values of n.[29] These results are purely local and limited to short wavelength perturbations. Therefore, they are not sufficient to obtain information on the most unstable global modes of the vortex. For this purpose, it is necessary to use a global theory and to interpret the instability in terms of Kelvin mode resonance. This constitutes the subject of the present paper which is organized as follows.

In Sec. II, it is shown that Kelvin mode resonance is possible only if $n=2$, 3 and 4 and a formal expression of the growth rate is obtained for $n=2$ and 3. In Sec. III, cases $n=2$ and 3 are treated quantitatively: the growth rate is computed for each resonant combination and the role of viscosity in the mode selection process is analyzed. Case $n=4$ is special, as the resonance occurs for infinite axial wave numbers. It requires a separate treatment, which is presented in Sec. IV. In Sec. V a physical explanation of the instability is provided in terms of vortex stretching. In particular, it is shown that the more unstable the mode combinations, the more important the correlation between perturbation vorticity and the direction of stretching of the basic flow. In the last section, the results are summarized and discussed in the context of turbulent flows.

II. INSTABILITY MECHANISM AND SCALINGS

In this section, the calculation of a formal expression for the growth rate of the instability is detailed. The presentation follows the papers of Tsai and Widnall[12] and Moore and Saffman.[13] However their analysis is extended to account for multipolar strain, general resonant modes and viscous effects. The linear equations for the perturbation of the deformed Rankine vortex are first given and the Kelvin modes are defined. Then the mechanism of Kelvin mode coupling with the multipolar strain field is described and analyzed in the limit of weak strain using perturbation theory.

A. Governing equations for the perturbations

Consider a linear perturbation of the basic flow Eqs. (1.1a), (1.1b) of small amplitude λ and assume, as in Tsai and Widnall,[12] that the perturbation is potential outside the vortex core. The perturbation is then defined by its velocity potential Φ outside the vortex core, its four-component velocity-pressure field $\mathbf{v}=(v_r;v_\theta;v_z;p)$ inside the vortex core and the displacement a of the vortex edge. Accordingly the core of the perturbed vortex is defined by $r \leq R+\lambda a$.

The equations for $\mathbf{v}$ are obtained by linearizing the Navier–Stokes equations around the vortex core expression (1.1a). They can be written in the following condensed form:

$$\frac{\partial}{\partial t}\mathcal{J}\mathbf{v}+\mathcal{M}\mathbf{v}=\varepsilon(e^{in\theta}\mathcal{N}+e^{-in\theta}\bar{\mathcal{N}})\mathbf{v}+\nu\mathcal{L}\mathbf{v}+O(\varepsilon^2), \quad (2.1)$$

where $\mathcal{J}$, $\mathcal{M}$, $\mathcal{N}$ and $\mathcal{L}$ are operators given in Appendix A. In Eq. (2.1), $\bar{\mathcal{N}}$ is the matrix whose elements are the complex conjugates of those in $\mathcal{N}$, and ν is the kinematic viscosity. Note that, with our nondimensionalization, the dimensionless viscosity ν is also the Ekman number of the flow based on the radius of the vortex core. Both parameter ε and viscosity ν are assumed to be small in the following. As seen below for $n=2$ and 3, the distinguished limit is obtained when both parameters are of same order. The rescaled viscosity $\nu_1=\nu/\varepsilon$ will indeed be the only control parameter in these cases. The equation for the velocity potential Φ outside the core is

$$\Delta\Phi=0. \quad (2.2)$$

For small ε, the equations for the edge displacement a follow from the kinematic and dynamic boundary conditions evaluated at $r=1$:

$$v_r-\frac{\partial\Phi}{\partial r}=\varepsilon \cos(n\theta)\left(v_\theta-\frac{\partial\Phi}{\partial\theta}\right)$$
$$-\frac{\varepsilon}{n}\sin(n\theta)\left(\frac{\partial v_r}{\partial r}-\frac{\partial^2\Phi}{\partial r^2}\right)+O(\varepsilon^2), \quad (2.3a)$$

$$v_r=\frac{\partial a}{\partial t}+\frac{\partial a}{\partial\theta}+O(\varepsilon), \quad (2.3b)$$

$$p+\frac{\partial\Phi}{\partial t}+\frac{\partial\Phi}{\partial\theta}=-\varepsilon \cos(n\theta)\frac{\partial\Phi}{\partial r}-\frac{\varepsilon}{n}\sin(n\theta)\left(-n\frac{\partial\Phi}{\partial\theta}\right.$$
$$\left.+\frac{\partial p}{\partial r}+\frac{\partial^2\Phi}{\partial r\partial t}+\frac{\partial^2\Phi}{\partial r\partial\theta}\right)+O(\varepsilon^2). \quad (2.3c)$$

The system of Eqs. (2.1)–(2.2) with the matching conditions Eqs. (2.3a)–(2.3c) describes the evolution of the linear perturbation $(\mathbf{v},a,\Phi)$ of the vortex in the limit of small strain.

B. Description of the Kelvin modes

As explained by Tsai and Widnall[12] and Moore and Saffman,[13] the instability of a deformed vortex patch is the consequence of the coupling of Kelvin modes with the external field. The Kelvin mode perturbations are defined as the inviscid normal modes of the underlying axisymmetric basic flow (i.e., the Rankine vortex). Thus, they satisfy Eqs. (2.1),
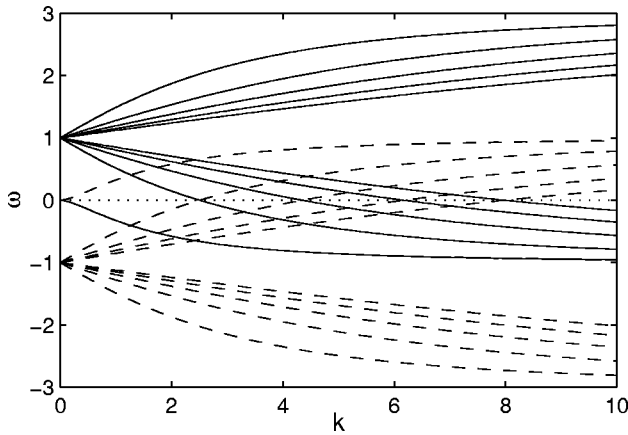
FIG. 2. Dispersion relation of the Kelvin modes in the (k,ω)-plane for $m=-1$ (dashed line) and $m=1$ (solid line). Only the first ten branches are represented.

(2.2), and (2.3a)–(2.3c) with $\varepsilon=\nu=0$. Their velocity-pressure field $\mathbf{v}_K$, edge displacement a_K and velocity potential Φ_K can be written as

$$\mathbf{v}_K(k,m,\omega)=\mathbf{U}(r)e^{i(kz+m\theta-\omega t)}+\text{c.c.},\qquad(2.4a)$$

$$a_K(k,m,\omega)=\rho e^{i(kz+m\theta-\omega t)}+\text{c.c.},\qquad(2.4b)$$

$$\Phi_K(k,m,\omega)=\phi(r)e^{i(kz+m\theta-\omega t)}+\text{c.c.},\qquad(2.4c)$$

where the axial wave number k, the azimuthal wave number m and the frequency ω are connected through a dispersion relation $D(k,m,\omega)=0$ which is obtained by enforcing conditions (2.3a) and (2.3c). The calculation leading to the dispersion relation $D(k,m,\omega)=0$ is classical[30] and will not be reproduced here. Expressions for $\mathbf{U}(r)$, ρ, $\phi(r)$ and $D(k,m,\omega)=0$ are given in Appendix A.

It is useful to emphasize a few important properties of the dispersion relation. For each azimuthal wave number m and axial wave number k, there is a discrete infinity of frequencies ω satisfying $D(k,m,\omega)=0$. They are all real and in the interval

$$m-2<\omega<m+2.\qquad(2.5)$$

In Fig. 2 the first branches of the dispersion relation are plotted in the (k,ω)-plane for $m=1$ and $m=-1$. Note that, when k goes to zero, all the branches accumulate to the frequency $\omega=m$ except a particular branch which tends to $\omega=m-\text{sgn}(m)$. This property is true for all $m\neq0$. For $m=0$, this particular branch does not exist.

C. Kelvin mode resonance and instability

The Kelvin modes are neutral. The Rankine vortex without external field is then expected to be marginally stable to vortex core perturbations. (A convincing proof of this statement is still lacking contrarily to what is claimed in Arendt et al.[31]) However, as explained by Moore and Saffman,[13] a small asymmetry is sufficient to couple Kelvin modes and may lead to exponential growth. The coupling term associated with the multipolar strain field is the first term on the right-hand side of Eq. (2.1). The azimuthal dependence $e^{\pm in\theta}$ of this term implies that only Kelvin modes of azimuthal

wave numbers separated by n can be coupled at leading order. The condition of resonance of two Kelvin modes (k_1,m_1,ω_1) and (k_2,m_2,ω_2), with $m_2>m_1$, is then

$$k_1=k_2,\quad m_2-m_1=n,\quad \omega_1=\omega_2.\qquad(2.6)$$

This condition of resonance is analyzed in the (k,ω)-plane by looking for the crossing points of the dispersion relations associated with two Kelvin modes of azimuthal wave numbers m_1 and m_2 separated by n. For $n=2$, this was done by Tsai and Widnall[12] for the two helical modes $m_1=-1$, $m_2=1$.

Here property Eq. (2.5) implies that resonance can occur only if $n=2$ or 3. For $n=4$, resonance is also possible for infinite axial wave numbers (as branches merge for $k\to\infty$); this case will be studied separately in Sec. IV. For $n\geqslant5$, the family of branches of two Kelvin modes of azimuthal wave numbers separated by n are totally distinct. Consequently, in such a case, no instability by a Kelvin mode resonance phenomenon is possible at leading order. This is in agreement with our previous result[29] that the flow is locally stable to small n-fold symmetrical deformation if $n\geqslant5$.

The end of the present section is dedicated to a formal calculation of the growth rate of a resonant Kelvin mode combination when $n=2$ or 3. The calculation closely follows Moore and Saffman's presentation.[13] We start with a perturbation $(\mathbf{v},a,\Phi)$ of the form

$$\mathbf{v}=[A_1\mathbf{U}^{(1)}(r)e^{im_1\theta}+A_2\mathbf{U}^{(2)}(r)e^{im_2\theta}$$
$$+\varepsilon\mathbf{v}_1(r,\theta)]e^{i(kz-\omega t)}e^{\varepsilon\sigma_1 t}+O(\varepsilon^2)+\text{c.c.},\qquad(2.7a)$$

$$a=[A_1\rho^{(1)}e^{im_1\theta}+A_2\rho^{(2)}e^{im_2\theta}+\varepsilon F_1]e^{i(kz-\omega t)}e^{\varepsilon\sigma_1 t}$$
$$+O(\varepsilon^2)+\text{c.c.},\qquad(2.7b)$$

$$\Phi=[A_1\phi^{(1)}(r)e^{im_1\theta}+A_2\phi^{(2)}(r)e^{im_2\theta}$$
$$+\varepsilon\Phi_1(r,\theta)]e^{i(kz-\omega t)}e^{\varepsilon\sigma_1 t}+O(\varepsilon^2)+\text{c.c.}\qquad(2.7c)$$

At leading order this perturbation is a combination of two resonant Kelvin modes (k,m_1,ω) and (k,m_2,ω) with unknown amplitudes A_1 and A_2. Therefore it is a leading order solution of equations (2.1), (2.2) and (2.3a)–(2.3c). The correction term $\varepsilon\mathbf{v}_1$ as well as the slowly varying factor $e^{\varepsilon\sigma_1 t}$ are generated by the right-hand side of Eq. (2.1). They are due to the interaction of Kelvin modes with the nonaxisymmetric part of the basic flow and to the viscous damping of the perturbation.

The frequency ω being real, the temporal growth rate of the resonant Kelvin modes is then given by $\sigma=\varepsilon\text{Re}(\sigma_1)$. In Tsai and Widnall,[12] σ is obtained by fully integrating Eqs. (2.1), (2.2) and (2.3a)–(2.3c) up to the order ε. Here we prefer to follow the simpler calculation of Moore and Saffman's[13] which is based on a solvability condition for $\mathbf{v}_1$. The form of the right-hand side of Eq. (2.1) indicates that $\mathbf{v}_1$ can be written as

$$\mathbf{v}_1=\mathbf{V}_1 e^{im_1\theta}+\mathbf{V}_2 e^{im_2\theta}+\mathbf{V}_3 e^{i(m_1-n)\theta}+\mathbf{V}_4 e^{i(m_2+n)\theta}.\qquad(2.8)$$

Inserting this expression in Eq. (2.1) gives for $\mathbf{V}_1$ and $\mathbf{V}_2$

$$(-i\omega\mathcal{J}+\mathcal{M}_{m_1})\mathbf{V}_1 = -A_1\sigma_1\mathcal{J}\,\mathbf{U}^{(1)}+A_1\nu_1\mathcal{L}_{m_1}\mathbf{U}^{(1)}$$

$$+A_2\bar{\mathcal{N}}_{m_2}\mathbf{U}^{(2)}, \tag{2.9a}$$

$$(-i\omega\mathcal{J}+\mathcal{M}_{m_2})\mathbf{V}_2 = -A_2\sigma_1\mathcal{J}\,\mathbf{U}^{(2)}+A_2\nu_1\mathcal{L}_{m_2}\mathbf{U}^{(2)}$$

$$+A_1\mathcal{N}_{m_1}\mathbf{U}^{(1)}, \tag{2.9b}$$

where the notation $\mathcal{M}_{m_1}$ means $\mathcal{M}_{m_1}=[\mathcal{M}e^{i(m_1\theta+kz)}]e^{-i(m_1\theta+kz)}$. The integration of these equations is not needed.

Introducing the following scalar product:

$$\langle\mathbf{X}|\mathbf{Y}\rangle = \int_0^1(\bar{X}_rY_r+\bar{X}_\theta Y_\theta+\bar{X}_zY_z+\bar{X}_pY_p)r\;dr, \tag{2.10}$$

the solvability condition is obtained by forming the scalar product of $\mathbf{U}^{(1)}$ and $\mathbf{U}^{(2)}$ with Eqs. (2.9a) and (2.9b), respectively. It leads to coupled amplitude equations for A_1 and A_2:

$$A_2I_1+A_1\sigma_1J_1 = -A_1\sigma_1\mathcal{J}_{1|1}+A_1\nu_1\mathcal{L}_{1|1}+A_2\bar{\mathcal{N}}_{1|2}, \tag{2.11a}$$

$$A_1I_2+A_2\sigma_1J_2 = -A_2\sigma_1\mathcal{J}_{2|2}+A_2\nu_1\mathcal{L}_{2|2}+A_1\mathcal{N}_{2|1}, \tag{2.11b}$$

where the following notation has been used:

$$\mathcal{N}_{2|1} = \langle\mathbf{U}^{(2)}|\mathcal{N}\mathbf{U}^{(1)}\rangle. \tag{2.12}$$

The coefficients I_1, I_2, J_1 and J_2 are boundary terms defined in $r=1$ by

$$I_1 = \frac{1}{2}P^{(1)}\left(U_\theta^{(2)}-\frac{i}{n}\frac{\partial U_r^{(2)}}{\partial r}-im_2\phi^{(2)}+\frac{i}{n}\frac{\partial^2\phi^{(2)}}{\partial r^2}\right)$$

$$-\frac{1}{2}\overline{U_r^{(1)}}\left(\frac{i}{n}\frac{\partial P^{(2)}}{\partial r}+m_2\phi^{(2)}+\frac{\omega-m_2+n}{n}\frac{\partial\phi^{(2)}}{\partial r}\right), \tag{2.13a}$$

$$I_2 = \frac{1}{2}P^{(2)}\left(U_\theta^{(1)}+\frac{i}{n}\frac{\partial U_r^{(1)}}{\partial r}-im_1\phi^{(1)}-\frac{i}{n}\frac{\partial^2\phi^{(1)}}{\partial r^2}\right)$$

$$+\frac{1}{2}\overline{U_r^{(2)}}\left(\frac{i}{n}\frac{\partial P^{(1)}}{\partial r}+m_1\phi^{(1)}+\frac{\omega-m_1-n}{n}\frac{\partial\phi^{(1)}}{\partial r}\right), \tag{2.13b}$$

$$J_1 = -\overline{U_r^{(1)}}\phi^{(1)}, \tag{2.13c}$$

$$J_2 = -\overline{U_r^{(2)}}\phi^{(2)}, \tag{2.13d}$$

where $U_r^{(1)}$, $U_r^{(2)}$ and $P^{(1)}$, $P^{(2)}$ are the radial velocity and pressure of the modes $\mathbf{U}^{(1)}$ and $\mathbf{U}^{(2)}$. These boundary terms come from the $O(\varepsilon)$ correction terms in the matching conditions Eqs. (2.3a)–(2.3c). Note that the external potential flow intervenes in the amplitude equations (2.11a),(2.11b) via the boundary terms I_1, I_2, J_1 and J_2 and the dispersion relation only.

The equation for the growth rate σ_1 is obtained by requiring that the determinant of the linear system Eqs. (2.11a),(2.11b) vanishes:
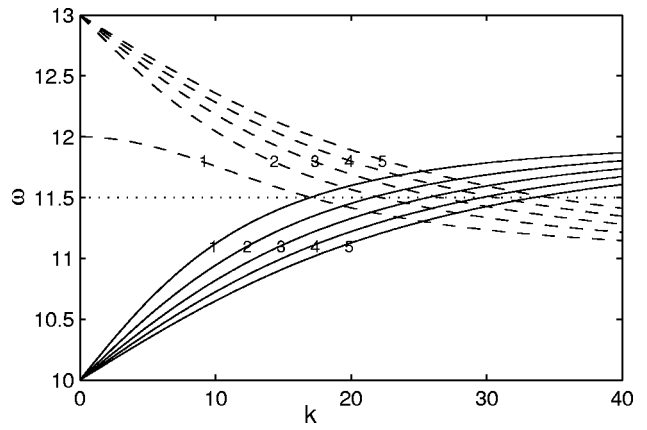

FIG. 3. Dispersion relation of the Kelvin modes in the (k,ω)-plane for $m_1=10$ (solid line) and $m_2=13$ (dashed line). The numbers label the different branches as explained in the text. The growth rates of the modes corresponding to the different intersection points are displayed in Table II.

$$[\sigma_1(\mathcal{J}_{1|1}+J_1)-\nu_1\mathcal{L}_{1|1}][\sigma_1(\mathcal{J}_{2|2}+J_2)-\nu_1\mathcal{L}_{2|2}]$$

$$=(\bar{\mathcal{N}}_{1|2}-I_1)(\mathcal{N}_{2|1}-I_2). \tag{2.14}$$

This relation is the formal expression of the growth rate we were looking for. For a given resonant Kelvin mode combination, the growth rate σ_1 only depends on the rescaled viscosity ν_1. Here, the difficulty is that the number of resonant Kelvin mode combination is doubly infinite. For each n, there is an infinity of possible couples of azimuthal wave numbers (m_1,m_2) which satisfy the relation $m_2-m_1=n$. And for a given couple (m_1,m_2), there exists as mentioned above infinitely many crossing points in the (k,ω)-plane. However the dispersion relation Eq. (A13) and Eq. (2.14) are invariant by the following symmetry: $(\omega,k,m_1,m_2)\rightarrow(-\omega,k,-m_1,-m_2)$. Therefore, the study can readily be restricted to mode combinations satisfying $m_1+m_2\geq0$.

In the next section, the different coefficients of Eq. (2.14) are computed for a large range of resonant Kelvin mode combination using the definitions of the operators given in Appendix A. In Appendix B, these coefficients are analytically evaluated in the limit of large k and large m.

III. DIPOLAR AND TRIPOLAR STRAIN FIELD ($n=2,3$)

This section focuses on the cases $n=2$ and $n=3$, for which the formal expression (2.14) for the growth rate applies. In a first subsection, the viscous damping is neglected which amounts to considering $\nu_1=0$. This permits to compare our expression with the previous results of Tsai and Widnall[12] and with the local and inviscid results obtained in Ref. 29. In a second subsection, the effect of viscosity is analyzed and the growth rate of the most unstable Kelvin mode combinations is computed as a function of ν_1.

A. Inviscid analysis

When $\nu_1=0$, Eq. (2.14) reduces to a simple expression for the inviscid growth rate:

$$\sigma_i^2 = \frac{(\bar{\mathcal{N}}_{1|2}-I_1)(\mathcal{N}_{2|1}-I_2)}{(\mathcal{J}_{1|1}+J_1)(\mathcal{J}_{2|2}+J_2)}\varepsilon^2. \tag{3.1}$$

TABLE I. Table of the computed inviscid growth rate σ_i/ε for $m_1=-1$, $m_2=1$ as a function of the branch label. The columns are the different branches of the dispersion relation for m_1 and the lines for m_2. The underlined growth rates are for the principal modes $(-1,1,2)$, $(-1,1,3)$, etc.

	1	2	3	4	5
1	–	0.0041	0.0046	0.0038	0.0031
2	0.0041	0.5708	0.0073	0.0061	0.0051
3	0.0046	0.0073	0.5695	0.0061	0.0053
4	0.0038	0.0061	0.0061	0.5681	0.0051
5	0.0031	0.0051	0.0053	0.0051	0.5672

For each m, we choose to label by an integer each branch of the dispersion relation in the order of increasing k (see Fig. 3). We computed expression (3.1) for 10 000 resonant Kelvin mode combinations (the combinations corresponding to the 100 crossing points of the first 10 branches of the dispersion relations of the azimuthal wave numbers m_1 and $m_2=m_1+n$ with $n=2$ and 3 and $-1\leqslant m_1\leqslant 48$). As an illustration, typical values of the growth rate σ_i/ε are given for the mode combinations $(m_1,m_2)=(-1,1)$ and $(m_1,m_2)=(10,13)$ in Tables I and II (for the crossing points displayed in Figs. 2 and 3).

In this computation, we observed that all resonant Kelvin mode combinations are unstable (i.e., σ_i is always real). We also found that, for $m_1\leqslant 48$, growth rates are significantly larger for the crossing points of branches with the same label. In the following, these combinations will be named *principal modes* and numbered using the notation

$$(m_1,m_2,i),\tag{3.2}$$

where i is the common label for m_1 and m_2. For $n=2$, $m_1=-1$, $m_2=1$, these crossing points are exactly on the axis of symmetry $\omega=0$ of the branch family (see Fig. 2). They are the resonant stationary helical modes studied by Tsai and Widnall[12] and Moore and Saffman.[13] The principal mode $(-1,1,1)$ of vanishing axial wave number correspond to a global translation of the vortex. As in Tsai and Widnall, it will be discarded in the following. For all the other cases, principal modes do not exhibit particular symmetries. Note that the first principal mode $(m_1,m_2,1)$ always involves the particular m_2 branch issued from the point $(k,\omega)=(0,m_2-1)$.

In Table III the axial wave numbers k of the first principal modes (m_1,m_1+n,i) are given. For given i and n, this axial wave number increases with m_1 and tends to ∞ as $m_1\to\infty$. The variations of the principal mode growth rate as a function of the axial wave number k are displayed in Fig. 4. Note that the graphs for $n=2$ [Fig. 4(a)] and $n=3$ [Fig.

TABLE II. Same as Table I for $m_1=10$, $m_2=13$. The boxed-in growth rate corresponds to the combination examined in Fig. 12.

	1	2	3	4	5
1	1.2658	0.1685	0.0681	0.0375	0.0236
2	0.3678	1.1049	0.0864	0.0458	0.0281
3	0.1514	0.3679	1.0220	0.0460	0.0319
4	0.0860	0.1292	0.3864	0.9657	0.0219
5	0.0561	0.0724	0.1191	0.4051	0.9242

TABLE III. Table of the axial wave numbers k of the most unstable modes (m_1,m_2,i) in the dipolar and tripolar cases, for $i\leqslant 4$.

	Dipolar		Tripolar		
i	$(-1,1,i)$	$(0,2,i)$	$(-1,2,i)$	$(0,3,i)$	$(1,4,i)$
1	0.0000	1.2422	2.2920	3.9360	5.3810
2	2.5050	3.3701	6.1719	7.8218	9.3722
3	4.3491	5.2264	9.7861	11.471	13.078
4	6.1740	7.0584	13.371	15.076	16.718

4(b)] are qualitatively different. For $n=2$, the inviscid growth rate is maximum for the combination $(-1,1,2)$. It asymptotes the limit value $(9/16)\varepsilon$ when $k\to\infty$ [dash-dotted lines in Fig. 4(a)]. For $n=3$, the growth rate is a decreasing function of k for fixed m_1 and reaches a limit value $49\varepsilon/(8\pi^2)\approx 0.62\varepsilon$ as $k\to\infty$ [lower dash-dotted lines in Fig. 4(b)]. As can be noticed in Fig. 4(b), this limit value is much smaller than the maximum growth rate $(49/32)\varepsilon\approx 1.53\varepsilon$ which is attained when $m_1\to\infty$ for fixed $i\neq 1$ (upper dash-dotted line).

In Sec. V, a physical interpretation will be given explaining why some modes have larger growth rates than others. The asymptotic analysis for large k and large m_1 that provides the limit values for $n=2$ and 3 are detailed in Ap-
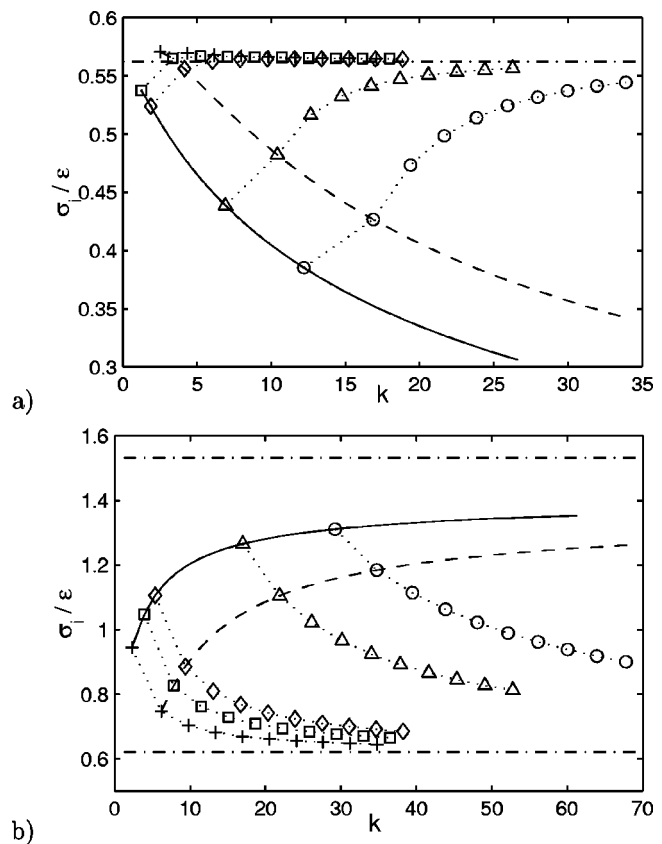

FIG. 4. Inviscid growth rates σ_i/ε for the principal modes (m_1,m_1+n,i) as a function of their axial wave number k for dipolar strain field $(n=2)$ (a) and tripolar strain field $(n=3)$ (b). In both cases, the symbols are: $+$: $m_1=-1$, $\square$: $m_1=0$, $\diamond$: $m_1=1$, $\triangle$: $m_1=10$, $\bigcirc$: $m_1=20$ and the solid and the dashed lines are the inviscid growth rate of the modes $(m_1,m_1+n,1)$ and $(m_1,m_1+n,2)$, respectively, for $-1\leqslant m_1\leqslant 48$. The dash-dotted lines are asymptotic values for large wave numbers: $\sigma_i=(9/16)\varepsilon$ in (a); $\sigma_i=49\varepsilon/(8\pi^2)$ and $\sigma_i=(49/32)\varepsilon$ in (b).

pendix B. The main results of this analysis are now summarized. In the limit of large k, for $n=2$, the asymptotic inviscid growth rate is proved to be maximum for principal modes. For other resonant combination, the growth rate tends to zero for large k. For $n=3$, the large k asymptotic growth rate is given by

$$\sigma_i = \frac{49\varepsilon}{8\pi^2(2i-2j-1)^2}, \tag{3.3}$$

where i and j are the branch labels for m_1 and m_2, respectively. This asymptotic growth rate is maximum not only for the principal modes ($i=j$) but also for the adjacent modes defined by the condition $i=j+1$. The asymptotic results for large m_1 are different. For both $n=2$ and $n=3$, the principal modes are no longer the most unstable modes. The growth rate of the first principal modes ($m_1,m_2,1$) even goes to zero as m_1 goes to infinity. The large m_1 asymptotic growth rate is now maximum for adjacent modes $i=j+1$ with $j \neq 1$. For $n=2$ this maximum is the same as the maximum large k asymptotic growth rate $(9/16)\varepsilon$. The situation is different for $n=3$. The maximum large m asymptotic growth rate $\sigma_i \approx 1.53\varepsilon$ is much larger than the maximum large k asymptotic growth rate $\sigma_i \approx 0.62\varepsilon$.

The results for $m_1=-1$ and $m_2=1$ (see Fig. 2 and Table I) can directly be compared to those of Tsai and Widnall.[12] The inviscid growth rates and axial wave numbers computed here are in agreement with their results for the principal modes $(-1,1,2)$ and $(-1,1,3)$. However, we found that all Kelvin mode combinations are unstable whereas Tsai and Widnall[12] found that some may be stable. A conclusion similar to ours has been reached by Vladimirov and Il'in[32] for the Kirchhoff vortex which makes us confident of our result. Note, however, that this discrepancy is not expected to strongly affect Tsai and Widnall's conclusions as the resonant combination they found stable are in fact amplified with a negligible growth rate (50 times smaller than the maximum growth rate).

The large wave number growth rates $(9/16)\varepsilon$ $(n=2)$ and $(49/32)\varepsilon$ $(n=3)$ correspond to the local maximum growth rates of the most unstable streamline in the vortex core.[29] This result was not guaranteed. Indeed, the dispersion relation for the Kelvin modes is a constraint on the axial and azimuthal wave numbers which is not present in the local stability analysis. Note, however, that the value of the local maximum growth rates are reached in the limit of large azimuthal and axial wave numbers for $n=3$ while only large axial wave number is needed for $n=2$. This could be related to the differences in the local stability properties for $n=2$ and $n=3$. For $n=2$ the local stability properties are the same for all streamlines in the vortex core while for $n=3$ the flow is not uniform and the most unstable streamline is located near the boundary where the strain rate is maximum. Thus, for $n=3$, resonant Kelvin mode combinations have to be localized near the boundary to be the most unstable and this occurs only for large m_1 as illustrated in Fig. 5. Note finally that the agreement with the local stability properties of the vortex core shows that the potential flow outside the
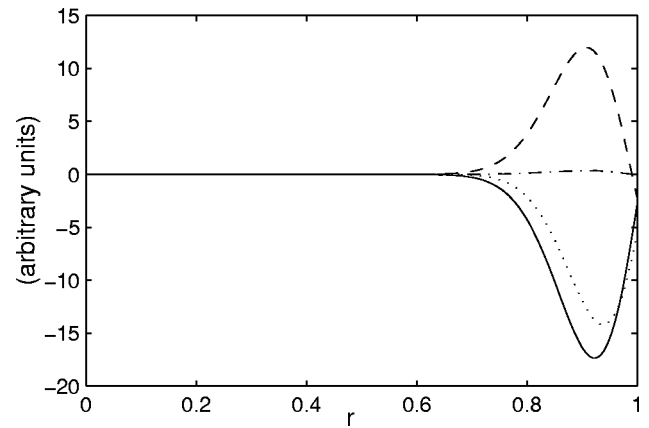

FIG. 5. Four components of the Kelvin mode $\mathbf{v}_K(k,m,\omega)$ $=\mathbf{U}(r)e^{i(kz+m\theta-\omega t)}$ for $m=39$, $\omega \approx 40.5$ and $k \approx 51.9$ (corresponding to a resonance with $m=42$). We have $\mathbf{U}=(iU;V;W;P)$ with U in the solid line, V in the dotted line, W in the dashed line and P in the dash-dotted line.

vortex has negligible influence on the stability results in the limit of large wave numbers.

B. Viscous selection process

In the previous section the maximum inviscid growth rate for $n=3$ was shown to asymptote its maximum value in the limit of a large azimuthal wave number. This is no longer expected to hold when viscosity is included, as viscous effects damp perturbations with large wave numbers. Moreover, we shall see below that, for $n=2$, another resonant combination than the principal mode $(-1,1,2)$ may become the most unstable in the viscous regime.

In the present paper, only volumic viscous effects on the perturbation are considered. In particular, we neglect the viscous diffusion of the basic flow as commonly done in stability analysis of inviscid solutions.[33] The effect of basic flow diffusion has been analyzed elsewhere.[34] In addition, the viscous effects on the perturbation due to the boundary layer at the edge of the vortex core are not considered. These effects[35] are $O(\nu^{1/2})$, but they are not strongly dependent on the perturbation wave number and therefore are not expected to influence the inviscid selection process. Moreover, these viscous layers are not present for more realistic vortices with continuous vorticity profile. It is then natural not to take into account these effects if one wants to obtain generic instability scenari. Note finally that both boundary layer effects and viscous diffusion effects are negligible if $k \gg \nu^{-1/4}$. The assumptions made here are therefore fully justified in the limit of large k.

In the growth rate expression Eq. (2.14), volumic viscosity effects appear via the terms $\nu_1 \mathcal{L}_{1|1}$ and $\nu_1 \mathcal{L}_{2|2}$. Each of these terms can roughly be decomposed into three parts: one proportional to k^2, another proportional to m_1^2 and a third one mostly connected to the geometrical character of the Kelvin modes. Thus, the viscous damping is of the form $-\nu_1 C_1 k^2 - \nu_1 C_2 m_1^2 + o(m_1^2, k^2)$ where C_1 and C_2 are two positive
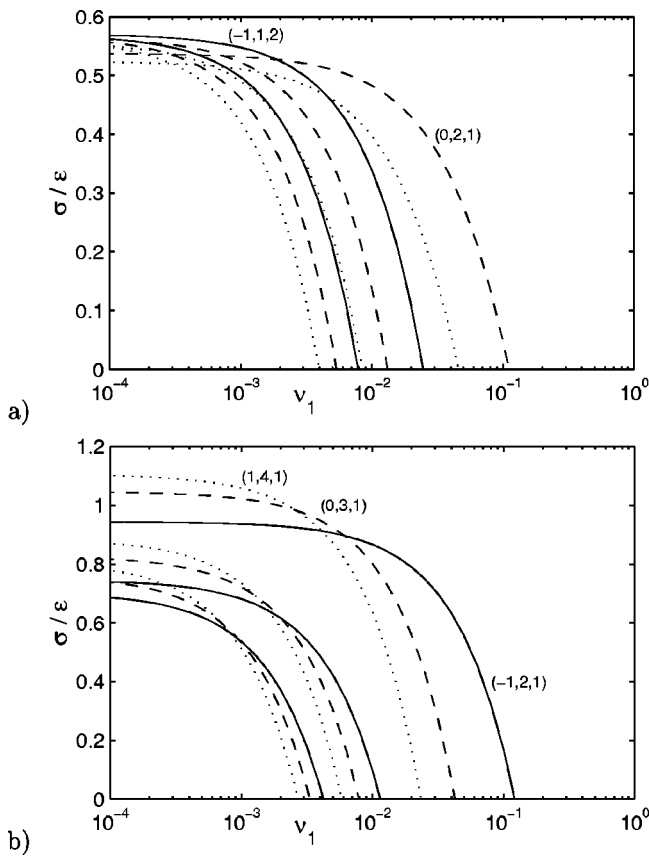
a)

b)

FIG. 6. Normalized growth rate of the principal modes (m_1, m_1+n, i) as a function of ν_1. (a) Dipolar strain $(n=2)$ and (b) tripolar strain $(n=3)$. Solid lines: $m_1=-1$, dashed lines: $m_1=0$ and dotted lines: $m_1=1$. Here, for the sake of legibility, only the first nine principal modes are plotted but the tendency is unchanged for higher modes $(i>3, m_1>1)$.

slowly varying functions of k and m_1. For a given viscosity, the viscous growth rate is then maximum for finite k and m_1. In other words, viscosity selects a particular resonant Kelvin mode combination.

The result of this selection process for $n=2$ and $n=3$ is illustrated in Fig. 6. In these figures, the viscous growth rate is computed as a function of ν_1 for the first principal modes (m_1, m_2, i) with $-1 \leqslant m_1 \leqslant 1$ and $1 \leqslant i \leqslant 3$. The principal modes are still the most unstable wave combinations when viscosity is added but it can be seen in Fig. 6 that the relative stability of one combination with respect to the others

changes with ν_1. For $n=2$, the most unstable Kelvin mode combination is $(-1,1,2)$ for small viscosity and $(0,2,1)$ for larger viscosity. This was expected from inviscid analysis since, among all other modes, mode $(-1,1,2)$ has the largest inviscid growth rate and mode $(0,2,1)$ has the smallest axial wave number. For $n=3$, the most unstable Kelvin mode combination is always a principal mode of the form $(m_1, m_1+3, 1)$ with m_1 increasing for decreasing ν_1. Again, the inviscid results are recovered when $\nu_1 \to 0$: the most unstable combination corresponds to modes with the infinite azimuthal wave number m_1.

For both $n=2$ and 3, there is a viscous cutoff ν_{1c} ($\nu_{1c} \simeq 0.111$ for $n=2$ and $\nu_{1c} \simeq 0.122$ for $n=3$) above which all Kelvin mode combinations are damped. For a dipolar strain field, this result can be compared to those obtained by Landman and Saffman.[36] Using a local approach, they found that there exists a critical Ekman number (here equal to the dimensionless viscosity ν), depending on the wave number of the perturbation and on the strain strength, above which the elliptic flow is stable. In the limit of small strain, Landman and Saffman's threshold reads $\nu_{1c} \simeq 0.131/k^2$ which becomes for the smallest resonant wave number (see Table III) $\nu_{1c} \simeq 0.084$. This estimate is within 25% from our value. Note, however, that Landman and Saffman's approach is unable to give estimates of the viscous damping for modes with a more complex azimuthal structure. In addition to the difference in the selected modes, one can also notice that there is a much larger variation of inviscid growth rates in case $n=3$ than in case $n=2$. The mode selection is then expected to be less efficient for $n=2$ and for small viscosity.

The structure of several resonant Kelvin mode combination is shown in Figs. 7(a), 7(b). The deformation of the vortex core by the perturbation has been depicted using Eq. (2.3b). For $n=2$, the combination $(-1,1,2)$ gives rise to an undulation of the vortex in the plane of maximal stretching [Fig. 7(a)]. This is in agreement with experimental observations.[14,16,23] For larger viscosity, the principal mode $(0,2,1)$ becomes the most unstable combination. The growth of this mode implies the bulging ($m_1=0$) and splitting ($m_2=2$) of the vortex core [see Fig. 7(b)]. This result is new and shows the limitation of the analysis of Tsai and Widnall[12] which only considered helical mode resonance. It will be discussed again in light of a recent numerical simulation[37] in Sec. VI. Note finally that for very small viscosity, the growth
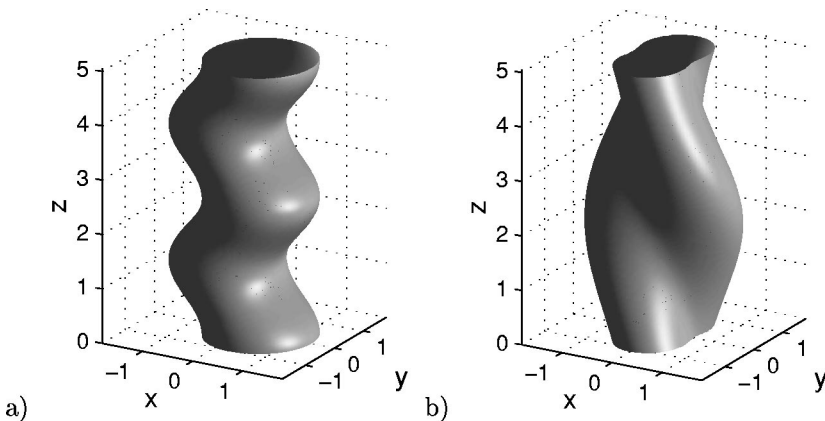

a)

b)

FIG. 7. Illustration of the Rankine vortex deformation induced by the principal modes $(-1,1,2)$ (a) and $(0,2,1)$ (b). The vortex core displacement is represented for perturbation amplitude equal to $\lambda=0.1$ and 0.2, respectively (with $A_1=1$).
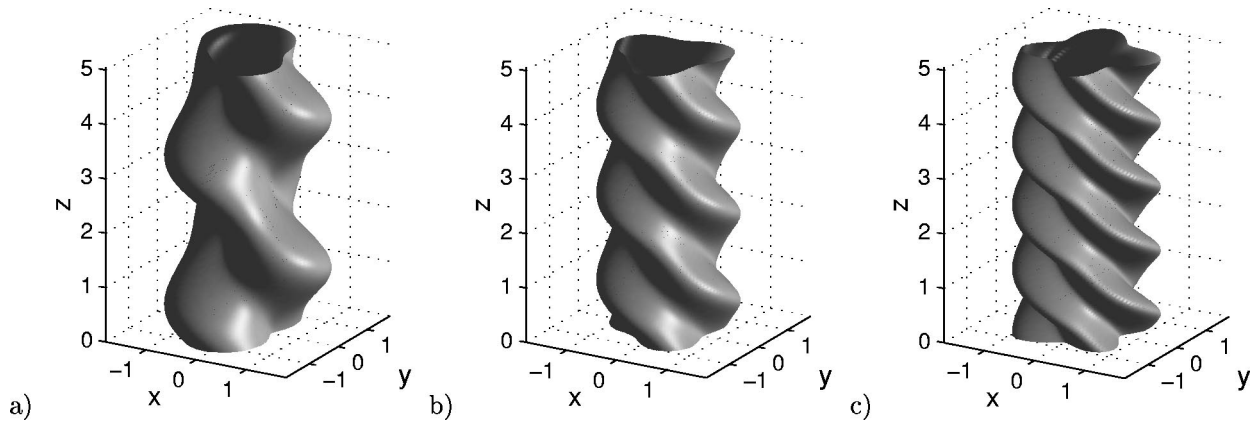
FIG. 8. Same as Fig. 7 for the principal modes $(-1,2,1)$ (a), $(0,3,1)$ (b) and $(1,4,1)$ (c) with $\lambda=0.2$, 0.1 and 0.1, respectively.

rate of most principal modes becomes comparable (within 2% for $\nu_1 < 10^{-4}$). Depending on the initial conditions, one could then imagine that modes with a more complex azimuthal structure could also develop. This would give a simple explanation of the rich dynamics of vortex filaments observed in large Reynolds number flows.

For $n=3$, the structure of the most unstable combination strongly depends on viscosity. Close to the threshold ν_{1c}, the most unstable mode is as illustrated in Fig. 8(a). When ν_1 is progressively decreased, the most unstable combination becomes more and more complex. It first gains a three-strand structure [Fig. 8(b)], then a four-strand structure [Fig. 8(c)], and so on.

IV. QUADRUPOLAR STRAIN FIELD ($n=4$)

In Secs. II and III, we considered the dipolar ($n=2$) and tripolar ($n=3$) strain fields for which there exist Kelvin mode resonances at finite axial wave numbers k. For the quadripolar strain field ($n=4$) such resonances do not exist, since $m-2<\omega<m+2$ for finite k. However, (k,m_1,ω) and (k,m_1+4,ω) may resonate for infinite k if $\omega=m_1+2$. In such a case, the resonant state is singular and the analysis of Sec. II does not apply. To treat this large k resonance, a specific asymptotic analysis is carried out in this section.

If the axial wave number k is large but not infinite, the resonance is imperfect and there is an offset of frequency for each Kelvin mode, which is deduced from Eq. (A11):

$$|\Delta\omega|=\delta^2/k^2. \tag{4.1}$$

The distinguished limit is obtained when this offset is of same order as the $O(\varepsilon)$ inviscid growth rate and the viscous damping rate. This corresponds to the scalings:

$$\frac{\delta}{k}=O(\sqrt{\varepsilon}), \quad \nu k^2=O(\varepsilon). \tag{4.2}$$

It is then useful to rescale the viscosity and axial wave number as follows:

$$\nu_2=\frac{\nu}{\varepsilon^2}, \quad k_{-1/2}=k\sqrt{\varepsilon}. \tag{4.3}$$

Following the analysis of Sec. II, the perturbation is then taken in the form

$$\mathbf{v}=[A_1(T)\mathbf{U}^{(1)}(r)e^{im_1\theta}e^{if^{(1)}T}+A_2(T)\mathbf{U}^{(2)}(r)e^{im_2\theta}e^{-if^{(2)}T}]$$
$$\times e^{i(kz-\omega t)}+\varepsilon\mathbf{v}_1(r,\theta,z,t), \tag{4.4}$$

where $A_1(T)$ and $A_2(T)$ are the amplitudes which vary on the slow time scale $T=\varepsilon t$, of the resonant Kelvin modes $\mathbf{v}_K(k,m_1,\omega-\varepsilon f^{(1)})$ and $\mathbf{v}_K(k,m_1+4,\omega+\varepsilon f^{(2)})$. We shall see below that, contrary to Sec. II, functions $A_1(T)$ and $A_2(T)$ are not necessarily exponentials of same argument. Expressions for $\mathbf{v}_K(k,m,\omega)$ are given in Eq. (A10). Note that, in this limit, $a\approx0$ and $\Phi\approx0$ such that the mode is localized in the core of the vortex. The frequency offsets $\Delta\omega=-\varepsilon f^{(1)}$ and $\Delta\omega=\varepsilon f^{(2)}$ depend, via relation (A11), on δ_1 and δ_2 which are obtained through the dispersion relation (A13):

$$-\delta_1 J'_{|m_1|}(\delta_1)+m_1 J_{|m_1|}(\delta_1)=0, \tag{4.5a}$$

$$\delta_2 J'_{|m_2|}(\delta_2)+m_2 J_{|m_2|}(\delta_2)=0. \tag{4.5b}$$

These implicit equations are solved numerically. Again, each equation has an infinite number of solutions which correspond to the different branches of the dispersion relation and which can be numbered by the branch label. The amplitude equations for A_1 and A_2 can be obtained by the same procedure as in Sec. II. They now have the form

$$-\mathcal{J}_{1|1}\frac{\partial A_1}{\partial T}+\nu_1\mathcal{L}_{1|1}A_1+\bar{\mathcal{N}}_{1|2}e^{i2fT}A_2=0, \tag{4.6a}$$

$$-\mathcal{J}_{2|2}\frac{\partial A_2}{\partial T}+\nu_1\mathcal{L}_{2|2}A_2+\mathcal{N}_{2|1}e^{-i2fT}A_1=0, \tag{4.6b}$$

with $2f=f^{(1)}+f^{(2)}$. The large k assumption allows the viscous terms to be reduced to their leading order expression: $\nu_1\mathcal{L}_{1|1}=-\nu_2 k^2_{-1/2}\mathcal{J}_{1|1}$ and $\nu_1\mathcal{L}_{2|2}=-\nu_2 k^2_{-1/2}\mathcal{J}_{2|2}$. This permits one to obtain simple expressions for A_1 and A_2:

$$A_1(T)=c_1\exp[(if+\sqrt{\sigma_0^2-f^2}-\nu_2 k^2_{-1/2})T], \tag{4.7a}$$

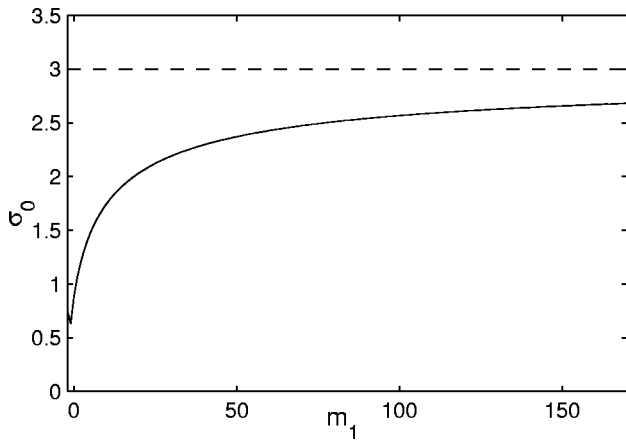$$A_2(T)=c_2\exp[(-if+\sqrt{\sigma_0^2-f^2}-\nu_2 k^2_{-1/2})T], \tag{4.7b}$$

with

FIG. 9. Stability of the Rankine vortex in a quadrupolar strain field. Maximum inviscid growth rate σ_0 of the principal modes $(m_1, m_1+4, 1)$ as a function of the azimuthal wave number m_1. The dashed line is the limit value for large m_1: $\sigma_0 = 3$.

$$\frac{c_2}{c_1} = \frac{\mathcal{N}_{2|1}}{\mathcal{J}_{2|2}(-if + \sqrt{\sigma_0^2 - f^2})}, \tag{4.8}$$

$$\sigma_0 = \frac{\mathcal{N}_{2|1} \bar{\mathcal{N}}_{1|2}}{\mathcal{J}_{1|1} \mathcal{J}_{2|2}}. \tag{4.9}$$

The growth rate of the resonant Kelvin mode combination then reads

$$\frac{\sigma}{\varepsilon} = \sqrt{\sigma_0^2 - f^2} - \nu_2 k_{-1/2}^2, \tag{4.10}$$

where f is a $O(1)$ function which depends on the labeled solutions $\delta_1(i)$ and $\delta_2(j)$ of Eqs. (4.5a),(4.5b):

$$f = \frac{\delta_1^2(i) + \delta_2^2(j)}{2k_{-1/2}^2}. \tag{4.11}$$

The first term in Eq. (4.10) is associated with inviscid effects only. Contrary to $n=2$ and $n=3$, there is a frequency cutoff: if $f^2 \geq \sigma_0^2$, the inviscid growth rate vanishes. This condition can be interpreted as a condition of resonance. Indeed, f measures the renormalized gap between the two Kelvin mode frequencies. If f is too large, there is no resonance anymore. Moreover, the inviscid growth rate is a decreasing function of f. As expected, it is maximum for a perfect resonance ($f = 0$) which occurs when $k = \infty$.

To determine the maximum growth rate, one has to compute $\delta_1(i)$ and $\delta_2(j)$ from Eqs. (4.5a),(4.5b) and the scalar products involved in Eq. (4.9). This computation was carried out for the range of parameters $-2 \leq m_1 \leq 170$, $i \leq 10$ and $j \leq 10$. The results can be summarized as follows. When $m_1 \geq 1$, σ_0 is maximum for the principal mode $(m_1, m_2, 1)$. Figure 9 shows the evolution of σ_0 for this mode as a function of m_1. Since f is an increasing function of the labels, other resonant Kelvin modes necessarily have a smaller growth rate. For $m_1 \geq 1$, then, the first principal mode is always the most unstable combination whatever $k_{-1/2}$ and ν_2. When $m_1 = -2$, -1 or 0, the first principal mode is the most unstable only if $k_{-1/2}$ is below a critical value k_c (k_c
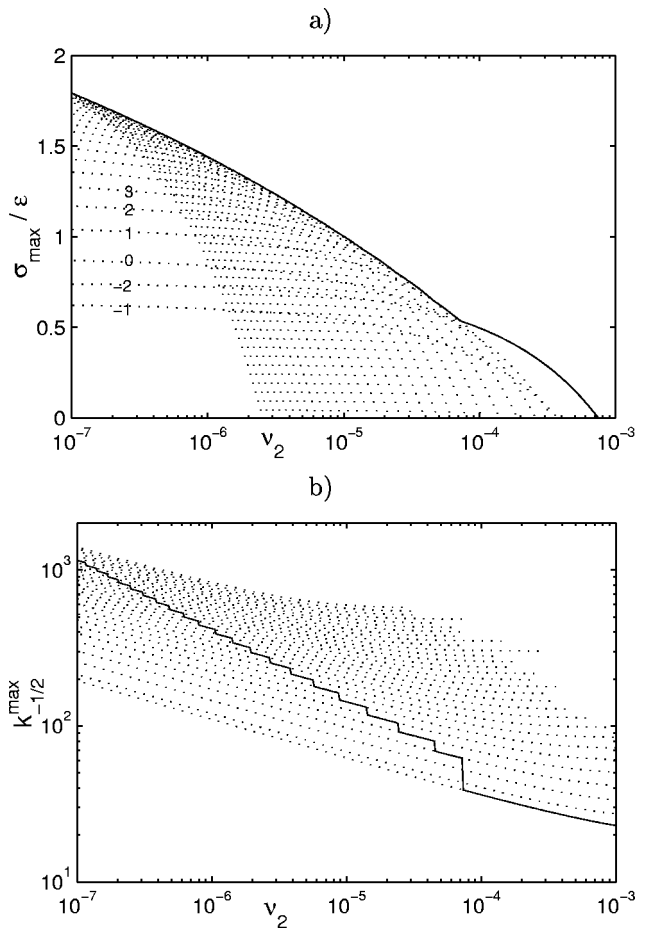

FIG. 10. Viscous effects on the instability characteristics of the Rankine vortex in a quadrupolar strain field. Growth rate σ_{max} (a) and corresponding axial wave number $k_{-1/2}^{max}$ (b) of the principal modes $(m_1, m_1+4, 1)$ as a function of ν_2. Each dotted line stands for a different azimuthal wave number as labeled on (a). On (b), m_1 is increasing from bottom to top. The solid line is the most unstable mode after a maximization over m_1.

$\simeq 89$, 56 and 1357 for $m_1 = -2$, -1 and 0, respectively). For $k_{-1/2} > k_c$, the maximum growth rate is always smaller than the growth rate of the first principal mode for $m_1 = 1$. Consequently the most unstable configuration is always a first principal mode of the form $(m_1, m_2, 1)$. Viscosity does not modify this conclusion. However, since it damps large wave number perturbations, it plays an important role in the wave number selection.

For fixed m_1 and ν_2, there exists an optimal wave number $k_{-1/2}^{max}$ which maximizes the growth rate $\sigma = \sigma_{max}$. Both σ_{max} and $k_{-1/2}^{max}$ are drawn in dotted lines as a function of ν_2 for different values of m_1 in Figs. 10(a) and 10(b), respectively. The solid line in Fig. 10(a) is the maximum growth rate among all possible m_1. The corresponding axial wave number is the solid line in Fig. 10(b). Despite the scaling difference, Fig. 10(a) exhibits the same features as Fig. 6(b) for $n = 3$: When viscosity is decreased below a critical value $\nu_{2c} \simeq 7.5 \times 10^{-4}$, the combination of modes with the smallest azimuthal wave number (here $m_1 = -2$, $m_2 = 2$) is first destabilized; then, combinations with higher m_1 progressively become the most unstable as $\nu_2 \to 0$. Note, however, that the principal modes $(-1,3,1)$ and $(0,4,1)$ are never the most

unstable for any ν_2. Note also that the first destabilized combination $m_1 = -2$, $m_2 = 2$ is stationary by symmetry as for $n = 2$.

As seen in Figs. 10(a) and 10(b), the most unstable combination when $\nu_2 \to 0$ has both a large $k_{-1/2}$ and a large m_1. A simplified expression of the growth rate can be obtained by asymptotic methods (as in Appendix B 2) in the large m_1 limit:

$$\frac{\sigma}{\varepsilon} = \sqrt{9 - \frac{m_1^4}{k_{-1/2}^4} - \nu_2 k_{-1/2}^2}. \tag{4.12}$$

For $\nu_2 = 0$ and $k_{-1/2} \to \infty$, the inviscid growth rate $\sigma_i = 3$ of the local stability analysis[29] is recovered.

V. PHYSICAL INTERPRETATION

In the previous sections, the instability was described as a resonance phenomenon of Kelvin modes due to the multipolar strain field. We computed the inviscid growth rate of the resonant combinations and noticed that there were important variations from one resonant configuration to the other. For large wave numbers, we showed that only very specific resonant configurations were significantly amplified. In this section, a physical interpretation is provided, which permits one to understand these variations and the inviscid selection of the most unstable resonant Kelvin mode configuration.

For this purpose, it is informative to first analyze the different terms in the linearized inner vorticity equation for the perturbations:

$$\frac{D\boldsymbol{\omega}}{Dt} = 2\frac{\partial \mathbf{u}}{\partial z} + \mathbf{e}_z \times \boldsymbol{\omega} + \mathcal{S}\boldsymbol{\omega}, \tag{5.1}$$

where $\boldsymbol{\omega}$ is the perturbation vorticity, $\mathbf{u}$ its velocity, D/Dt is the convective derivative and $\mathcal{S}$ is the strain tensor of the inner basic flow given by (in cylindrical coordinates)

$$\mathcal{S} = \varepsilon(n-1)r^{n-2} \begin{pmatrix} \cos(n\theta) & -\sin(n\theta) & 0 \\ -\sin(n\theta) & -\cos(n\theta) & 0 \\ 0 & 0 & 0 \end{pmatrix}. \tag{5.2}$$

The first term on the right-hand side of Eq. (5.1) represents the tilting and the stretching of the basic flow vorticity $\boldsymbol{\omega}_0 = 2\mathbf{e}_z$ by the perturbation. The second and third terms are, respectively, the tilting and the stretching of the perturbation vorticity by the basic flow. The role of each term in the instability has been discussed in various places (see, for instance, Refs. 22,24,38). Orszag and Patera[24] showed that the first term alone, or the second term and the third term taken together, cannot lead to exponential instability. In contrast, the third term alone is sufficient for instability as it provides exponential growth of the vorticity component aligned with the direction of stretching[22] (principal axis of the strain tensor $\mathcal{S}$ with the largest positive strain rate). Here, in addition, one can show that the first and second terms taken together do not provide instability. Indeed, these terms are associated with a solid body rotation [$\varepsilon = 0$ in Eq. (1.1a)]: The normal mode solutions are, in that case, nothing more than the neutral Kelvin modes studied above.

Outside the vortex core, both basic flow and Kelvin modes have zero vorticity so no amplification can be generated in this potential region. However, in the vortex core, Kelvin modes exhibit vorticity components in the (x,y) plane (in Cartesian coordinates) where the stretching term [third term in Eq. (5.1)] acts. Therefore these vorticity components can be amplified by stretching when they are aligned with the direction of stretching. In order to study this possibility, we shall now evaluate the correlation between the direction of stretching and the direction of the vorticity projected onto the (x,y) plane for a given Kelvin mode and for a combination of two resonant Kelvin modes.

The local stretching rate $s(r)$ and the local direction of stretching $\varphi_s(\theta)$ are defined from $\mathcal{S}$ as the positive eigenvalue and the direction of the associated eigenvector $\mathbf{e}_s$. Here, they are given by

$$s(r) = \varepsilon(n-1)r^{n-2}, \tag{5.3}$$

$$\varphi_s(\theta) = -n\theta/2, \tag{5.4}$$

where the angle φ_s is measured in the local polar basis [i.e., $\cos(\varphi_s) = \mathbf{e}_s \cdot \mathbf{e}_r$]. For $n = 2$, the stretching rate and the direction of stretching ($\mathbf{e}_s = \mathbf{e}_x$) are uniform. For larger n, there are both a radial dependence of the stretching rate and an angular dependence of the stretching direction.

The projected vorticity $\boldsymbol{\omega}_\perp$ of the Kelvin mode $\mathbf{v}_K(k,m,\omega)$ is obtained from formulas (A10a)–(A10d). It takes the form

$$\boldsymbol{\omega}_\perp = f(r)\sin\psi\,\mathbf{e}_r + g(r)\cos\psi\,\mathbf{e}_\theta, \tag{5.5}$$

where

$$\psi = kz + m\theta - \omega t, \tag{5.6}$$

and f and g are real functions of r. The direction of this vector is then given (in the local polar basis) by a formula of the form

$$\varphi_{\boldsymbol{\omega}_\perp}(r,\theta,z,t) = \arctan\left(\frac{g(r)}{f(r)}\frac{1}{\tan\psi}\right). \tag{5.7}$$

Similarly, for a combination of two Kelvin modes $\mathbf{v}_{K1}(k_1,m_1,\omega_1) + \mathbf{v}_{K2}(k_2,m_2,\omega_2)$ we get

$$\varphi_{\boldsymbol{\omega}_\perp} = \arctan\left(\frac{g_1(r)\cos\psi_1 + g_2(r)\cos\psi_2}{f_1(r)\sin\psi_1 + f_2(r)\sin\psi_2}\right), \tag{5.8}$$

with

$$\psi_1 = k_1 z + m_1\theta - \omega_1 t, \tag{5.9}$$

$$\psi_2 = k_2 z + m_2\theta - \omega_2 t. \tag{5.10}$$

It is important to note the dependence of ψ on kz, $m\theta$ or ωt in Eq. (5.6). For fixed r and θ, this dependence implies that $\varphi_{\boldsymbol{\omega}_\perp}$, for a single Kelvin mode, takes all possible values as t or z varies and has a mean value independent of θ, whereas φ_s is θ periodic. The result is that there is no mean correlation between the direction of stretching φ_s and the direction of the projected vorticity $\varphi_{\boldsymbol{\omega}_\perp}$ for a single Kelvin mode. This is reassuring as a single Kelvin mode was not expected to be unstable in a planar strain field.
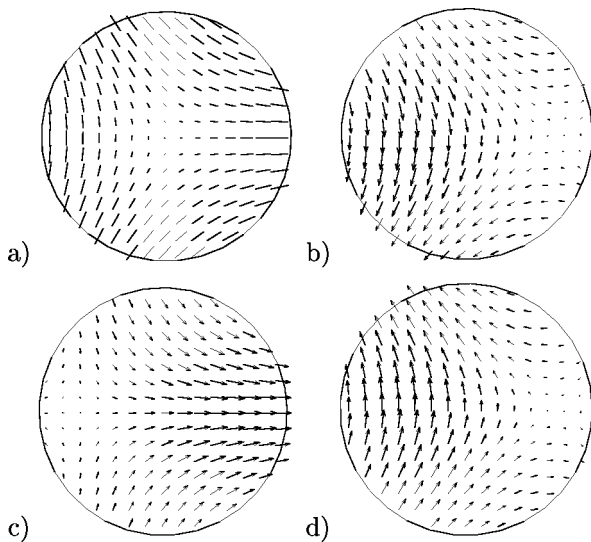
FIG. 11. Example of good correlation between stretching and vorticity direction for an unstable mode of the Rankine vortex in a tripolar strain field ($n=3$). Local direction and intensity of stretching (a) and projected vorticity in the (x,y)-plane of the principal mode $(-1,2,1)$ in $z=0$ (b), $z=\pi/2k$ (c) and $z=\pi/k$ (d).
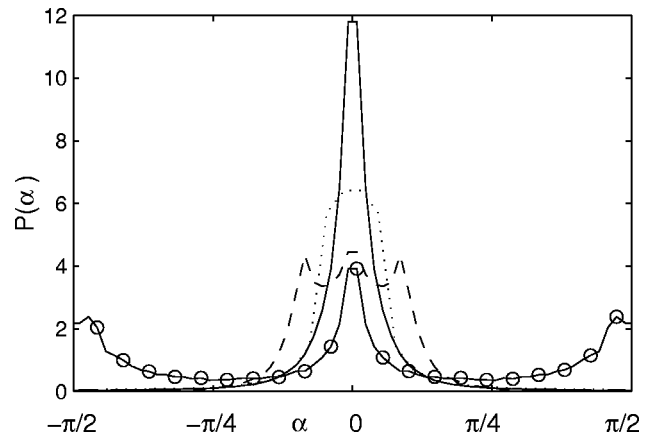

FIG. 12. Distribution of the angle α between the direction of the vorticity in the (x,y)-plane and the direction of stretching for the principal modes $(-1,2,1)$ (solid line), $(-1,1,2)$ (dashed line), $(1,5,1)$ (dotted line) and a mode with $m_1=10$, $m_2=13$ but taking the resonant crossing point of the first and third branches, respectively ($\bigcirc$) (the boxed in mode of Table II).

However, for a two Kelvin mode combination, the above argument does not always apply because cancellation in Eq. (5.8) is now possible. In particular, $\varphi\boldsymbol{\omega}_\perp$ may have a nonzero mean value dependent on θ at particular values of r if the two modes have same axial wave number ($k_1=k_2$) and the same frequency ($\omega_1=\omega_2$). If this occurs and if $\varphi\boldsymbol{\omega}_\perp=\varphi_s$ for a specific location at any time, the planar component of vorticity is locally amplified by stretching at that position with a growth rate equal to $s(r)$. Accordingly, the maximum growth rate of the perturbation is always bound by the maximum local stretching rate of the strain field [here $(n-1)\varepsilon$]. This upper bound corresponds to a pointwise maximum growth rate. It should not be mixed with the local maximum growth rate obtained in Ref. 29 which is a mean growth rate along a closed streamline: In general, the local maximum growth rate is smaller because the perturbation vorticity is not aligned with the stretching direction on the whole streamline. Case $n=4$ is an exception: both local and pointwise maximum growth rates are equal in that case. Moreover, we saw in Sec. IV that this maximum is also reached by the growth rate of the most unstable resonant Kelvin mode combination in the large m_1 and k limit. This can be explained by the fact that, in this limit, the projected vorticity of the perturbation is localized in the region of maximum stretching rate (close to $r=1$) and is everywhere aligned with the stretching direction.

For the other unstable Kelvin mode combinations, the correlation is not perfect but exists as illustrated in Fig. 11. This figure displays the projected vorticity of the principal mode $(-1,2,1)$ (see Sec. III for the notation), which is unstable in a tripolar strain field ($n=3$). This combination clearly has its vorticity preferentially oriented along the direction of stretching associated with the triangular distortion. This alignment is quantified in Fig. 12 where the distribution of $\alpha=\varphi\boldsymbol{\omega}_\perp-\varphi_s$ is plotted for different resonant modes with the norm of the projected vorticity $\|\boldsymbol{\omega}_\perp\|$ as the weight of each point. These curves exhibit a peak near $\alpha=0$ for the unstable modes $(-1,1,2)$, $(-1,2,1)$ and $(1,5,1)$ indicating a strong correlation between the stretching direction and the vorticity. For a ''nonprincipal'' mode, for instance the one associated with the first and third branches of the dispersion relation for $m_1=10$ and $m_2=13$, respectively, this peak is smaller and there is a secondary peak at $\alpha=\pm\pi/2$. The correlation is then weaker and the inviscid growth rate much smaller ($\sigma_i=0.0681\varepsilon$ from Table I), as expected.

These graphs and the above discussion demonstrate that the mechanism of instability is directly related to the local stretching of perturbation vorticity by the basic flow. It confirms that the most unstable modes are those which maximize the alignment of their projected vorticity with the local direction of stretching. Moreover, for both $n=3$ and 4, we have seen above that the most unstable combinations tend to be localized near the vortex core edge where the stretching rate in the core is maximum.

Why principal modes are the configurations which maximize the alignment of vorticity and stretching is another issue. First, note that these configurations have a frequency ω approximatively equal to $(m_1+m_2)/2$ so that the ''radial wave numbers'' δ_1 and δ_2 of the resonant Kelvin modes [given by formula Eq. (A11)] are close to each other. This is clearly visible in the large wave number analysis of Appendix B, where the most unstable modes have been found to satisfy $\delta_1=\delta_2$ at leading order. Therefore, principal modes tend to be more coherent radially than the other modes which could explain why they are the most unstable. A more complete explanation has been recently given by Le Dizès.[39] He showed that the additional condition $\delta_1\approx\delta_2$ directly results from the characteristics of the most unstable local modes. In particular, for the elliptical case ($n=2$), he successfully justified why the local maximum growth rate is reached when this condition is satisfied. Figure 13 illustrates the clear correlation of small values of $|\delta_2-\delta_1|$ with a large inviscid growth rate for particular combinations of modes.
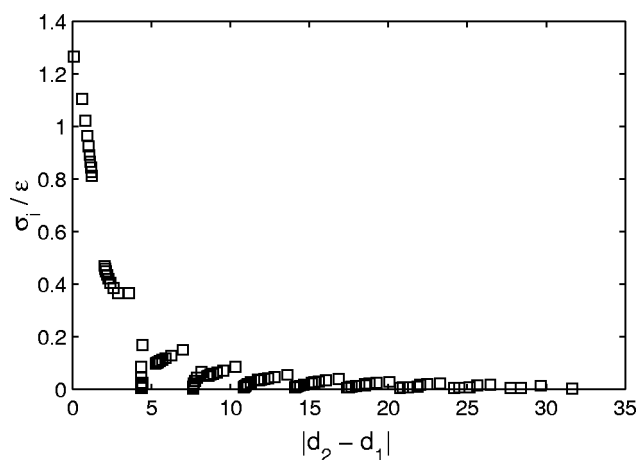
FIG. 13. Inviscid growth rate as a function of the difference $|\delta_2 - \delta_1|$ between the radial wave numbers of the two Kelvin modes $m_1 = 10$ and $m_2 = 13$ for the first 100 crossing points.

VI. DISCUSSION

In this paper, the linear stability of the Rankine vortex in a weak multipolar strain field was analyzed. This basic flow was shown to be subject to a Kelvin mode resonance instability for dipolar ($n = 2$), tripolar ($n = 3$) and quadrupolar ($n = 4$) strain fields. The unstable modes are combinations of two Kelvin modes of the same axial wave number, the same frequency, and azimuthal wave numbers separated by n. A physical interpretation of the instability in terms of local vorticity stretching was also provided. We demonstrated that the most unstable modes correspond to the modes for which the alignment between the projected vorticity and the direction of stretching is maximized. Viscous effects were also discussed in detail. The critical viscosity above which all Kelvin mode combinations are damped was computed in each case. Below this critical value, viscous effects were shown to select a preferential instability mode. For $n = 2$, we proved that the selected mode is a combination of stationary helical modes ($m_1 = -1$, $m_2 = 1$) if viscosity is sufficiently small. However, for larger viscosity, a combination of modes $m_1 = 0$ and $m_2 = 2$ become the most unstable. This unstable Kelvin mode combination has never been studied before. It is associated with the bulging–splitting of the vortex. For $n = 3$, the selected mode is a time-periodic Kelvin mode combination with both frequency, axial and azimuthal wave numbers increasing as viscosity decreases. For $n = 4$, the Kelvin mode resonance occurs only for large axial wave numbers, so viscosity must be smaller for instability in that case. However, as for $n = 3$, the selected mode was shown to have a more intricate azimuthal structure as the viscosity decreases.

For vortices with continuous vorticity profiles, instability by Kelvin mode resonance is also known to exist. In particular, Moore and Saffman showed that the stationary resonance of helical modes $m_1 = -1$ and $m_1 = 1$ is not dependent on a particular profile and generically leads to the instability of an elliptically perturbed vortex. Robinson and Saffman[40] also showed numerically that for finite strain [$\varepsilon = O(1)$], the stability of these particular symmetric modes is qualitatively well-described by a weak-strain analysis. However, all studies have restricted the analysis to the stability of these $m = \pm 1$ modes[12,13,32,40] arguing that other modes should be less unstable. In the present paper, we have shown that this restriction is not justified for the Rankine vortex as the most unstable mode for high viscosity is the principal mode $(0,2,1)$ corresponding to filament bulging–splitting. In a recent paper, Billant et al.[37] demonstrated that this bulging–splitting mode was indeed present for a Lamb–Chaplygin vortex pair. For Stuart vortices, they also suggested that the higher order mode, which is briefly discussed by Pierrehumbert and Widnall,[41] and the bulging mode (or the so-called Core Dynamics Instability mode) examined in Ref. 42 could be related to the principal mode $(0,2,1)$. However, in these three studies, the growth rate of this mode is approximatively half as small as the growth rate of $(-1,1,i)$ modes (bending or translative modes). In the present paper, they are almost equal. We have no explanation for this discrepancy except that, in each of these numerical cases, vortices are strongly deformed and the vorticity is strongly nonhomogeneous.

To our knowledge, for n-fold symmetry of higher order ($n \geqslant 3$), no result concerning the stability is available. This is due to the fact that the condition of resonance cannot be simplified by symmetry as was done by Moore and Saffman.[13] In principle, for $n = 2$, 3 or 4, the condition of resonance must be analyzed on a case-by-case basis for all modes different from the symmetric principal modes $(-1,1,i)$ and $(-2,2,i)$. Note, however, that once resonance occurs between two neutral Kelvin modes, the above analysis can be formally applied almost without modification. In particular, we expect the main conclusions to hold, i.e.:

(1) Instability for $n = 2$ and $n = 3$ for a viscosity smaller than an $O(\varepsilon)$ critical value and for $n = 4$ for viscosity smaller than an $O(\varepsilon^2)$ critical value;
(2) stability for $n \geqslant 5$ and small ε;
(3) the most unstable Kelvin mode combination changes as viscosity varies; and
(4) for vanishing viscosity, the most unstable Kelvin mode combination corresponds to the configuration for which vortex stretching is maximized.

Considering the similarities between the experimental and numerical observations of vortex filament destabilization[1,2,5] and the form of a vortex subject to a Kelvin mode resonance, it is natural to discuss the implications of the present results in the context of turbulent flows. In turbulence, vortex filaments are strained by the background turbulent flow or surrounding vortices. As there is no particular symmetry, they are in general elliptically deformed in their core. From the present analysis, we argue that if viscosity is small enough compared to the nonaxisymmetry of the filament ($\nu < 0.111\varepsilon$), the vortex can be subject to a Kelvin mode resonance instability. We showed that the most unstable mode was, in such a case, either the combination of two helical modes $(-1,1,2)$, which produces a planar undulation of the vortex, or the combination of a bulging and

splitting mode $(0,2,1)$ leading to the formation of strands on the filament. This behavior was observed in experiments[1] and in numerical simulations.[5]

In contrast, this instability does not explain the bursting of vortex filaments which is sometimes observed.[1] Pradeep *et al.*[43] gave an explanation which could be related to a secondary instability of the vortex deformed by Kelvin modes. Lifschitz *et al.*[44] first showed that this secondary instability indeed exists for elliptical flows. Recently, Kerswell[45] and Mason and Kerswell[46] studied this instability analytically and numerically in a configuration similar to that in Malkus' experiment.[14] In this elliptic cylinder geometry, it appears that the principal modes $(-1,1,2)$, $(-1,1,3)$ and $(0,2,1)$ are unstable and that the growth rate of the secondary instability is of the same order as the primary instability. Secondary instability analysis has never been carried out for a vortex in an open flow configuration but one would expect that the results of Kerswell[45,46] to remain qualitatively unchanged.

ACKNOWLEDGMENTS

APPENDIX A: NOTATIONS

The operators appearing in Eq. (2.1) are defined by

$$
\mathcal{J}=\begin{pmatrix} 1 & 0 & 0 & 0 \\ 0 & 1 & 0 & 0 \\ 0 & 0 & 1 & 0 \\ 0 & 0 & 0 & 0 \end{pmatrix}, \tag{A1}
$$

$$
\mathcal{M}=\begin{pmatrix} \dfrac{\partial}{\partial\theta} & -2 & 0 & \dfrac{\partial}{\partial r} \\[2mm] 2 & \dfrac{\partial}{\partial\theta} & 0 & \dfrac{1}{r}\dfrac{\partial}{\partial\theta} \\[2mm] 0 & 0 & \dfrac{\partial}{\partial\theta} & \dfrac{\partial}{\partial z} \\[2mm] \dfrac{\partial}{\partial r}+\dfrac{1}{r} & \dfrac{1}{r}\dfrac{\partial}{\partial\theta} & \dfrac{\partial}{\partial z} & 0 \end{pmatrix}, \tag{A2}
$$

$$
\mathcal{N}=\frac{1}{2}\begin{pmatrix} D_1-(n-1)r^{n-2} & -i(n-2)r^{n-2} & 0 & 0 \\ -inr^{n-2} & D_1+(n-1)r^{n-2} & 0 & 0 \\ 0 & 0 & D_1 & 0 \\ 0 & 0 & 0 & 0 \end{pmatrix}, \tag{A3}
$$

with

$$
D_1=-r^{n-1}\frac{\partial}{\partial r}-ir^{n-2}\frac{\partial}{\partial\theta}, \tag{A4}
$$

$$
\mathcal{L}=\Delta=\begin{pmatrix} D_2-\dfrac{1}{r^2} & -\dfrac{2}{r^2}\dfrac{\partial}{\partial\theta} & 0 & 0 \\[2mm] \dfrac{2}{r^2}\dfrac{\partial}{\partial\theta} & D_2-\dfrac{1}{r^2} & 0 & 0 \\[2mm] 0 & 0 & D_2 & 0 \\[2mm] 0 & 0 & 0 & 0 \end{pmatrix}, \tag{A5}
$$

and

$$
D_2=\frac{1}{r}\frac{\partial}{\partial r}+\frac{\partial^2}{\partial r^2}+\frac{1}{r^2}\frac{\partial^2}{\partial\theta^2}+\frac{\partial^2}{\partial z^2}. \tag{A6}
$$

The relation

$$
\mathcal{N}=\mathcal{A}+\mathcal{B}+\mathcal{C}, \tag{A7}
$$

is also used in Appendix B, where

$$
\mathcal{A}=\tfrac{1}{2}lr^{n-2}\mathcal{J}, \tag{A8a}
$$

$$
\mathcal{B}=-\frac{1}{2}r^{n-1}\frac{\partial}{\partial r}\mathcal{J}, \tag{A8b}
$$

$$
\mathcal{C}=\frac{1}{2}\begin{pmatrix} -(n-1)r^{n-2} & -i(n-2)r^{n-2} & 0 & 0 \\ -inr^{n-2} & (n-1)r^{n-2} & 0 & 0 \\ 0 & 0 & 0 & 0 \\ 0 & 0 & 0 & 0 \end{pmatrix}. \tag{A8c}
$$

The velocity–pressure field of the Kelvin mode in the vortex core is defined by

$$
\mathbf{v}_K(k,m,\omega)=\mathbf{U}(r)e^{i(kz+m\theta-\omega t)}+\text{c.c.}, \tag{A9}
$$

where $\mathbf{U}=(U_r;U_\theta;U_z;P)$ is given by

$$
U_r(r)=-i\left[(m-\omega)\delta J'_{|m|}(\delta r)+\frac{2m}{r}J_{|m|}(\delta r)\right], \tag{A10a}
$$

$$
U_\theta(r)=2\delta J'_{|m|}(\delta r)+\frac{m(m-\omega)}{r}J_{|m|}(\delta r), \tag{A10b}
$$

$$
U_z(r)=-\frac{k}{m-\omega}[4-(m-\omega)^2]J_{|m|}(\delta r), \tag{A10c}
$$

$$
P(r)=[4-(m-\omega)^2]J_{|m|}(\delta r), \tag{A10d}
$$

with J_μ as the Bessel function of the first kind and J'_μ its derivative. The scalar δ in these expressions is the "radial wave number" and is defined as

$$
\delta^2=\frac{k^2(2+m-\omega)(2-m+\omega)}{(m-\omega)^2}. \tag{A11}
$$

Amplitudes ρ and $\phi(r)$ of the displacement a_K and potential Φ_K of the Kelvin modes are

$$
\rho=\frac{i}{\omega-m}U_r(1), \tag{A12a}
$$

$$
\phi(r)=i\frac{4-(m-\omega)^2}{m-\omega}\frac{J_{|m|}(\delta)}{K_{|m|}(k)}K_{|m|}(kr). \tag{A12b}
$$

The dispersion relation $D(k,m,\omega)=0$ is given by

$$D(k,m,\omega)=(m-\omega)\,\delta J'_{|m|}(\delta)+2mJ_{|m|}(\delta)$$
$$+\frac{4-(m-\omega)^2}{m-\omega}\frac{K'_{|m|}(k)}{K_{|m|}(k)}kJ_{|m|}(\delta),\qquad(A13)$$

where K_μ is a modified Bessel function and K'_μ its derivative.

APPENDIX B: INVISCID ASYMPTOTICS ANALYSIS

In this appendix the inviscid growth rate of the resonant Kelvin mode combination is obtained by an asymptotic analysis in the limit of large axial wave number k and in the limit of large azimuthal wave number m. Our goal is first to calculate the limit values observed in Figs. 6 and 10, and then to check that they are in agreement with the local short wavelength analysis.[29] For this purpose, asymptotic expressions for the Kelvin modes are used to evaluate the various coefficients of the expression Eq. (3.1) of the inviscid growth rate σ_i.

1. Large k analysis

In this part, the azimuthal wave number m of the Kelvin mode is $O(1)$; the limit $m\to\infty$ will be analyzed in the next section. A simple expression for the Kelvin mode may be obtained by using asymptotic estimates for the Bessel functions J_μ, K_μ and their derivatives:

$$J_m(x)\sim\sqrt{\frac{2}{\pi x}}c_m(x)\quad\text{as }x\to\infty,\qquad(B1a)$$

$$J'_m(x)\sim-\sqrt{\frac{2}{\pi x}}s_m(x)\quad\text{as }x\to\infty,\qquad(B1b)$$

$$K_m(x)\sim\sqrt{\frac{\pi}{2x}}e^{-x}\quad\text{as }x\to\infty,\qquad(B1c)$$

where

$$c_m(x)=\cos\left(x-(2m+1)\frac{\pi}{4}\right),\qquad(B2a)$$

$$s_m(x)=\sin\left(x-(2m+1)\frac{\pi}{4}\right).\qquad(B2b)$$

In particular, this gives, when $\delta\to\infty$ and $\omega\neq m$ in the dispersion relation (A13),

$$\delta\sim l\pi+(2m+1)\frac{\pi}{4}-\arctan\frac{(16-n^2)k}{n^2\delta},\qquad(B3)$$

where l is a large integer which labels the branches. Note that l is directly related to the branch label i introduced in Sec. III by a relation of the form: $l-i=f(m)$. As also noticed in that section, one expects the largest growth rate to be obtained for the resonant Kelvin mode of same label i. It is then natural to assume that the radial wave numbers δ_1 and δ_2 of the two resonant Kelvin modes $\mathbf{v}_K(k,m_1,\omega)$ and $\mathbf{v}_K(k,m_2,\omega)$ are of the same order. This leads to

$$\omega\sim(m_1+m_2)/2,\qquad(B4a)$$

$$\frac{\delta}{k}\sim\frac{\sqrt{16-n^2}}{n}.\qquad(B4b)$$

This expression, in addition to Eqs. (B1a)–(B1c), allows one to estimate the scalar products appearing in Eq. (3.1). Upon writing $\mathcal{N}_{2|1}=\mathcal{A}_{2|1}+\mathcal{B}_{2|1}+\mathcal{C}_{2|1}$ with the definition Eqs. (A8a)–(A8c) for $\mathcal{A}$, $\mathcal{B}$ and $\mathcal{C}$, we get, after a careful estimation of each term,

$$I_1\sim I_2\sim\frac{8-n^2}{4\pi}\delta_1 s_{m_1}(\delta_1)s_{m_2}(\delta_2),\qquad(B5a)$$

$$J_1\sim J_2\ll\delta_1,\qquad(B5b)$$

$$\mathcal{J}_{1|1}\sim\mathcal{J}_{2|2}\sim\frac{8}{\pi}\delta_1,\qquad(B5c)$$

$$\mathcal{A}_{2|1}\sim-\bar{\mathcal{A}}_{1|2}\ll\delta_1,\qquad(B5d)$$

$$\mathcal{B}_{2|1}\sim\bar{\mathcal{B}}_{1|2}\sim I_1.\qquad(B5e)$$

The last term $\mathcal{C}_{2|1}$ has two different expressions for $n=2$ and $n=3$:

$$\mathcal{C}_{2|1}\sim\bar{\mathcal{C}}_{1|2}\sim\frac{9}{2\pi}\int_0^{\delta_1}\cos\left(\frac{\delta_1-\delta_2}{\delta_1}x\right)dx$$
$$\sim\begin{vmatrix}\frac{9}{2\pi}\delta_1 & \text{if }\delta_1=\delta_2\\[4pt]o(\delta_1) & \text{if }\delta_1\neq\delta_2\end{vmatrix},\quad\text{for }n=2,\qquad(B6a)$$

$$\mathcal{C}_{2|1}\sim\bar{\mathcal{C}}_{1|2}\sim\frac{49}{4\pi\delta_1}\int_0^{\delta_1}x\cos\left(\frac{\delta_1-\delta_2}{\delta_1}x+\frac{3\pi}{2}\right)dx$$
$$\sim\frac{49}{4\pi}\delta_1\frac{\sin(\delta_1-\delta_2)}{(\delta_1-\delta_2)^2},\quad\text{for }n=3.\qquad(B6b)$$

The expression Eq. (3.1) then reduces to

$$\sigma_i\sim\frac{|\mathcal{C}_{2|1}|}{\mathcal{J}_{1|1}}\varepsilon.\qquad(B7)$$

This gives

$$\sigma_i\sim\begin{vmatrix}\frac{9}{16}\varepsilon & \text{if }\delta_1=\delta_2\\[4pt]o(\varepsilon) & \text{if }\delta_1\neq\delta_2\end{vmatrix}\quad\text{for }n=2,\qquad(B8a)$$

$$\sigma_i\sim\frac{49\varepsilon}{32(\delta_1-\delta_2)^2}\quad\text{for }n=3.\qquad(B8b)$$

Besides, for $n=3$, using expression Eq. (B3), $\delta_1-\delta_2=(l_1-l_2)\pi-(3\pi/2)$, which implies that the maximum $\sigma_{i(\max)}=49\varepsilon/(8\pi^2)\simeq0.62\varepsilon$ is attained for $|\delta_1-\delta_2|=\pi/2$.

2. Large m analysis

In the limit of large m, the modified Bessel function $K_{|m|}$ satisfies

$$\frac{K'_{|m|}(k)}{K_{|m|}(k)}\sim-\frac{|m|}{k}\left(1+\frac{k^2}{m^2}\right)^{1/2}.\qquad(B9)$$

Therefore, the dispersion relation Eq. (A13) reduces to

$$-(\omega-m)^2\,\delta J'_{|m|}(\delta)+\left[2l(\omega-m)+|m|(4-(\omega-m)^2)\right.$$

$$\left.\times\left(1+\frac{k^2}{m^2}\right)^{1/2}\right]J_{|m|}(\delta)=0. \tag{B10}$$

a. First case ($\delta_1 \sim \delta_2 \sim m_1$)

If $\delta\sim m$, the Bessel function satisfies $J'_{|m|}(\delta)\ll J_{|m|}(\delta)$ and the dispersion relation is simplified. This corresponds to the branches of the dispersion relation for which $\omega=m$ in $k=0$ (see Fig. 3). The case which involves the particular branch leaving from $\omega=m-1$ is treated below. The adequate asymptotic expression for the Bessel function [see formula (9.3.23) of Abramowitz and Stegun's book[47]] is

$$J_l(m+\xi m^{1/3})\sim\frac{2^{1/3}}{m^{1/3}}\mathrm{Ai}(-2^{1/3}\xi)[1+O(m^{-2/3})]$$

$$+\frac{2^{2/3}}{m}\mathrm{Ai}'(-2^{1/3}\xi)\left[\frac{3}{10}z^2+O(m^{-2/3})\right], \tag{B11}$$

as $m\to\infty$ with fixed ξ and where Ai is the Airy function. The condition of resonance Eq. (2.6) of two Kelvin modes for $n=2$ and $n=3$ implies that at leading order

$$\omega\sim\frac{m_1+m_2}{2}, \tag{B12a}$$

$$k\sim\frac{\sqrt{16-n^2}}{n}m_1. \tag{B12b}$$

Inserting Eqs. (B12a),(B12b) in the dispersion relation Eq. (B10) also gives

$$\delta_1\sim m_1-\frac{a_1}{2^{1/3}}m_1^{1/3}+\frac{n^2}{4\sqrt{16-n^2}+4n}, \tag{B13a}$$

$$\delta_2\sim m_2-\frac{a_2}{2^{1/3}}m_2^{1/3}+\frac{n^2}{4\sqrt{16-n^2}-4n}, \tag{B13b}$$

where a_1, a_2 are $O(1)$ zeroes of the Airy function.

Here the branches are labeled by the zeroes of the Airy function. Let us first consider the case $a_1=a_2$. In that case, the scalar products appearing in Eq. (3.1) reduce to

$$\mathcal{J}_{1|1}\sim8Z_1, \tag{B14a}$$

$$\mathcal{J}_{2|2}\sim8Z_2, \tag{B14b}$$

$$J_1\sim J_2\ll m^{2/3}, \tag{B14c}$$

$$I_1\sim-\left(\frac{7}{8}-\frac{63\sqrt{7}}{32}\right)\sqrt{Z_1Z_2}, \tag{B14d}$$

$$I_2\sim-\left(\frac{7}{8}+\frac{63\sqrt{7}}{32}\right)\sqrt{Z_1Z_2}, \tag{B14e}$$

$$\mathcal{A}_{2|1}\sim-\bar{\mathcal{A}}_{1|2}\sim-\frac{63\sqrt{7}}{32}\sqrt{Z_1Z_2}, \tag{B14f}$$

$$\mathcal{B}_{2|1}\sim\bar{\mathcal{B}}_{1|2}\sim-\frac{7}{8}\sqrt{Z_1Z_2}, \tag{B14g}$$

$$\mathcal{C}_{2|1}\sim\bar{\mathcal{C}}_{1|2}\sim-\frac{49}{4}\sqrt{Z_1Z_2}, \tag{B14h}$$

where

$$Z_1=2^{1/3}m^{2/3}\,\mathrm{Ai}'^2(a_1), \tag{B15a}$$

$$Z_2=2^{1/3}m^{2/3}\,\mathrm{Ai}'^2(a_2), \tag{B15b}$$

and $\mathcal{N}=\mathcal{A}+\mathcal{B}+\mathcal{C}$. This leads to

$$\sigma_i\sim\frac{49}{32}\varepsilon, \quad\text{for }n=3. \tag{B16}$$

A similar calculation yields

$$\sigma_i\sim\frac{9}{16}\varepsilon, \quad\text{for }n=2. \tag{B17}$$

When $a_1\neq a_2$, the inviscid growth rate of the resonant Kelvin mode is smaller. An upper bound is obtained using the following relations (valid only for $a_1\neq a_2$):

$$\int_0^\infty\mathrm{Ai}(x+a_1)\mathrm{Ai}(x+a_2)\mathrm{d}x=0, \tag{B18a}$$

$$\int_0^\infty\mathrm{Ai}''(x+a_1)\mathrm{Ai}'(x+a_2)dx$$

$$=\left(\frac{a_1}{a_2-a_1}+\frac{6}{(a_2-a_1)^3}\right)\mathrm{Ai}'(a_1)\mathrm{Ai}'(a_2). \tag{B18b}$$

Relation Eq. (B18a) yields

$$\mathcal{C}_{2|1}\sim\bar{\mathcal{C}}_{1|2}\ll m^{2/3}. \tag{B19}$$

Equations (B14a)–(B14e) are still valid, so that, using identity Eq. (B18b),

$$(\bar{\mathcal{B}}_{1|2}-I_1)(\mathcal{B}_{2|1}-I_2)<\left(\frac{91}{24}2^{1/3}m^{2/3}\,\mathrm{Ai}'(a_1)\mathrm{Ai}'(a_2)\right)^2. \tag{B20}$$

It immediately follows that

$$\sigma_i<\frac{91}{192}\varepsilon. \tag{B21}$$

Then, for these modes, the inviscid growth rate is roughly three times smaller than the maximum growth rate. Case $a_1=a_2$, which maximizes the growth rate, corresponds to the branch crossing points $i=j+1$ where i and j are the branch label for m_1 and m_2, respectively.

b. Second case ($\delta_2 \sim Zm_2$ with $Z\neq1$)

This second case corresponds to the crossing points of the particular branch of the dispersion relation for m_2 and the regular branches for m_1. In particular, it corresponds to

modes $(m_1, m_1+n, 1)$ in the limit of large m_1. The scaling $\delta_1 \sim m_1$ still holds but $\omega \neq (m_1+m_2)/2$. The asymptotic expansion of the Bessel function leads to

$$\frac{J'_{|m|}(\delta_2)}{J_{|m|}(\delta_2)} \sim \frac{\sqrt{1-Z^2}}{Z} \quad \text{for } Z<1, \tag{B22a}$$

$$\frac{J'_{|m|}(\delta_2)}{J_{|m|}(\delta_2)} \sim \frac{\sqrt{Z^2-1}}{Z} \tan\left(\frac{\pi}{4} - |m|\sqrt{Z^2-1} + |m|\arccos\frac{1}{Z}\right)$$

$$\text{for } Z>1, \tag{B22b}$$

with $Z = \delta_2/m$. Using the asymptotic dispersion relation Eq. (B10) yields an implicit equation for Z which can be solved numerically. It follows that $m_2 - \omega \simeq 1.115$ for $n=2$ and $m_2 - \omega \simeq 1.496$ for $n=3$.

For both cases $n=2$ and 3, $m_2 - \omega \neq n/2$. This leads in the limit of large azimuthal wave numbers to an inviscid asymptotic growth rates $\sigma_i \ll \varepsilon$. However, for $n=3$, $m_2 - \omega$ is sufficiently close to $n/2$ to allow an unstable resonance for large m_1 but still $O(1)$. This explains why the modes $(m_1, m_1+3, 1)$ can remain the most unstable for the first m_1.

[1] O. Cadot, S. Douady, and Y. Couder, ''Characterization of the low pressure filaments in three-dimensional turbulent shear flow,'' Phys. Fluids **7**, 630 (1995).

[2] A. Vincent and M. Meneguzzi, ''The spatial structure and statistical properties of homogeneous turbulence,'' J. Fluid Mech. **225**, 1 (1991).

[3] J. Jiménez and A. A. Wray, ''On the characteristics of vortex filaments in isotropic turbulence,'' J. Fluid Mech. **373**, 255 (1998).

[4] J. Jiménez, A. A. Wray, P. G. Saffman, and R. S. Rogallo, ''The structure of intense vorticity in homogeneous isotropic turbulence,'' J. Fluid Mech. **255**, 65 (1993).

[5] S. Arendt, D. C. Fritts, and Ø. Andreassen, ''Kelvin twist waves in the transition to turbulence,'' Eur. J. Mech. B/Fluids **17**, 595 (1998).

[6] Lord Kelvin, ''Vibrations of a columnar vortex,'' Philos. Mag. **10**, 155 (1880).

[7] L. Ting and C. Tung, ''Motion and decay of a vortex in a nonuniform stream,'' Phys. Fluids **8**, 1039 (1965).

[8] H. K. Moffatt, S. Kida, and K. Ohkitani, ''Stretched vortices—The sinews of turbulence; large-Reynolds-number asymptotics,'' J. Fluid Mech. **259**, 241 (1994).

[9] J. Jiménez, H. K. Moffat, and C. Vasco, ''The structure of the vortices in freely decaying two dimensional turbulence,'' J. Fluid Mech. **313**, 209 (1996).

[10] S. E. Widnall and J. P. Sullivan, ''On the stability of vortex rings,'' Proc. R. Soc. London, Ser. A **332**, 335 (1973).

[11] S. E. Widnall, D. Bliss, and C.-Y. Tsai, ''The instability of short waves on a vortex ring,'' J. Fluid Mech. **66**, 35 (1974).

[12] C.-Y. Tsai and S. E. Widnall, ''The stability of short waves on a straight vortex filament in a weak externally imposed strain field,'' J. Fluid Mech. **73**, 721 (1976).

[13] D. W. Moore and P. G. Saffman, ''The instability of a straight vortex filament in a strain field,'' Proc. R. Soc. London, Ser. A **346**, 413 (1975).

[14] W. V. R. Malkus, ''An experimental study of global instabilities due to tidal (elliptical) distortion of a rotating elastic cylinder,'' Geophys. Astrophys. Fluid Dyn. **48**, 123 (1989).

[15] E. B. Gledzer and V. M. Ponomarev, ''Instability of bounded flows with elliptical streamlines,'' J. Fluid Mech. **240**, 1 (1992).

[16] T. Leweke and C. H. K. Williamson, ''Cooperative elliptic instability of a vortex pair,'' J. Fluid Mech. **360**, 85 (1998).

[17] T. Leweke and C. H. K. Williamson, ''Three-dimensional instabilities in wake transition,'' Eur. J. Mech. B/Fluids **17**, 571 (1998).

[18] R. T. Pierrehumbert, ''Universal short-wave instability of two-dimensional eddies in an inviscid fluid,'' Phys. Rev. Lett. **57**, 2157 (1986).

[19] B. J. Bayly, ''Three-dimensional instability of elliptical flow,'' Phys. Rev. Lett. **57**, 2160 (1986).

[20] A. Lifschitz and E. Hameiri, ''Local stability conditions in fluid dynamics,'' Phys. Fluids A **3**, 2644 (1991).

[21] B. J. Bayly, D. D. Holm, and A. Lifschitz, ''Three-dimensional stability of elliptical vortex columns in external strain flows,'' Philos. Trans. R. Soc. London, Ser. A **354**, 895 (1996).

[22] F. Waleffe, ''On the three-dimensional instability of strained vortices,'' Phys. Fluids A **2**, 76 (1990).

[23] Y. L. Chernous'ko, ''An experimental study of secondary multi-eddy flows in elliptical cylinders,'' Izv. Akad. Nauk SSSR FAO **14**, 151 (1978).

[24] S. A. Orszag and A. T. Patera, ''Secondary instability of wall-bounded shear flows,'' J. Fluid Mech. **128**, 347 (1983).

[25] B. J. Bayly, S. A. Orszag, and T. Herbert, ''Instability mechanisms in shear-flow transition,'' Annu. Rev. Fluid Mech. **20**, 359 (1988).

[26] H. C. Kuhlmann, M. Wanschura, and H. J. Rath, ''Elliptic instability in two-sided lid-driven cavity flow,'' Eur. J. Mech. B/Fluids **17**, 561 (1998).

[27] T. S. Lundgren and N. M. Mansour, ''Transition to turbulence in an elliptic vortex,'' J. Fluid Mech. **307**, 43 (1996).

[28] D. W. Moore and P. G. Saffman, ''Structure of a line vortex in an imposed strain,'' in *Aircraft Wake Turbulence and its Detection*, edited by J. H. Olsen, A. Goldburg, and M. Rogers (Plenum, New York, 1971), p. 339.

[29] S. Le Dizès and C. Eloy, ''Short-wavelength instability of a vortex in a multipolar strain field,'' Phys. Fluids **11**, 500 (1999).

[30] P. G. Saffman, *Vortex Dynamics* (Cambridge University Press, England, 1992).

[31] S. Arendt, D. C. Fritts, and Ø. Andreassen, ''The initial value problem for Kelvin vortex waves,'' J. Fluid Mech. **344**, 181 (1997).

[32] V. A. Vladimirov and K. I. Il'in, ''Three-dimensional instability of an elliptic Kirchhoff vortex,'' Mech. Zhid. Gasa **3**, 40 (1988).

[33] P. G. Drazin and W. H. Reid, *Hydrodynamic Stability* (Cambridge University Press, England, 1981).

[34] C. Eloy and S. Le Dizès, ''Three-dimensional instability of Burgers and Lamb-Oseen vortices in a strain field,'' J. Fluid Mech. **378**, 145 (1999).

[35] H. P. Greenspan, *The Theory of Rotating Fluids* (Cambridge University Press, England, 1968).

[36] M. J. Landman and P. G. Saffman, ''The three-dimensional instability of strained vortices in a viscous fluid,'' Phys. Fluids **30**, 2339 (1987).

[37] P. Billant, P. Brancher, and J.-M. Chomaz, ''Three dimensional stability of a vortex pair,'' Phys. Fluids **11**, 2069 (1999).

[38] P. Huerre and M. Rossi, ''Hydrodynamic instabilities in open flows,'' in *Hydrodynamics and Nonlinear Instabilities* (Cambridge University Press, England, 1998).

[39] S. Le Dizès, ''Three-dimensional instability of a multipolar vortex in a rotating flow,'' Phys. Fluids **12**, 2762 (2000).

[40] A. C. Robinson and P. G. Saffman, ''Three-dimensional stability of an elliptical vortex in a straining field,'' J. Fluid Mech. **142**, 452 (1984).

[41] R. T. Pierrehumbert and S. E. Widnall, ''The two- and three-dimensional instabilities of a spatially periodic shear layer,'' J. Fluid Mech. **114**, 59 (1982).

[42] W. Schoppa, F. Hussain, and R. W. Metcalfe, ''A new mechanism of small-scale transition in a plane mixing layer: Core dynamics of spanwise vortices,'' J. Fluid Mech. **298**, 23 (1995).

[43] D. S. Pradeep, F. Hussain, and W. Schoppa, ''Core dynamics instability of a vortex in a shear: A proto-typical cascade mechanism,'' Bull. Am. Phys. Soc. **42**, 2166 (1997).

[44] A. Lifschitz, T. Miyazaki, and B. Fabijonas, ''A new class of instabilities of rotating flows,'' Eur. J. Mech. B/Fluids **17**, 605 (1998).

[45] R. R. Kerswell, ''Secondary instabilities in rapidly rotating fluids: Inertial wave breakdown,'' J. Fluid Mech. **382**, 283 (1999).

[46] D. M. Mason and R. R. Kerswell, ''Nonlinear evolution of the elliptical instability: An example of inertial breakdown,'' J. Fluid Mech. **396**, 73 (1999).

[47] M. Abramowitz and I. A. Stegun, *Handbook of Mathematical Functions* (Dover, New York, 1965).